Article

Cell

Succinate Dehydrogenase Supports Metabolic Repurposing of Mitochondria to Drive Inflammatory Macrophages

Graphical Abstract

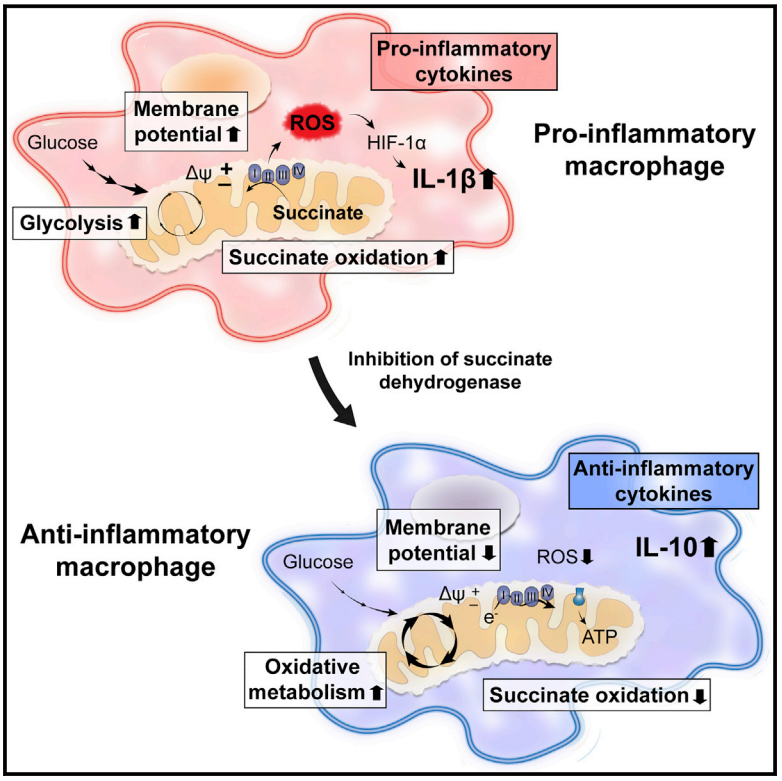

Authors

Evanna L. Mills, Beth Kelly, Angela Logan, ..., Christian Frezza, Michael P. Murphy, Luke A. O'Neill

Correspondence

mpm@mrc-mbu.cam.ac.uk (M.P.M.), laoneill@tcd.ie (L.A.O.)

In Brief

To support their pro-inflammatory function, activated macrophages repurpose their mitochondria, switching from ATP production to ROS generation.

Highlights

- LPS induces mitochondrial repurposing from ATP synthesis to ROS production
- Oxidation of succinate and mitochondrial hyperpolarization drive ROS production
- Blocking LPS-induced ROS production or hyperpolarization inhibits IL-1β
- SDH is critical for the inflammatory response

Data Resources

GSE78849

Mills et al., 2016, Cell *167*, 457–470
October 6, 2016 Crown Copyright © 2016 Published by Elsevier Inc.
http://dx.doi.org/10.1016/j.cell.2016.08.064

Article

Cell

Succinate Dehydrogenase Supports Metabolic Repurposing of Mitochondria to Drive Inflammatory Macrophages

Evanna L. Mills,[1,12,13] Beth Kelly,[1,12] Angela Logan,[2] Ana S.H. Costa,[3] Mukund Varma,[4] Clare E. Bryant,[6] Panagiotis Tourlomousis,[6] J. Henry M. Däbritz,[7] Eyal Gottlieb,[7] Isabel Latorre,[4] Sinéad C. Corr,[8] Gavin McManus,[1] Dylan Ryan,[1] Howard T. Jacobs,[9,10] Marten Szibor,[9,10,11] Ramnik J. Xavier,[4,5] Thomas Braun,[11] Christian Frezza,[3] Michael P. Murphy,[2,*] and Luke A. O'Neill[1,14,*]

[1]School of Biochemistry and Immunology, Trinity Biomedical Sciences Institute, Trinity College Dublin, Dublin 2, Ireland
[2]MRC Mitochondrial Biology Unit, Hills Road, Cambridge CB2 0XY, UK
[3]MRC Cancer Unit, University of Cambridge, Hutchison/MRC Research Centre, Box 197, Cambridge Biomedical Campus, Cambridge CB2 0XZ, UK
[4]Center for Computational and Integrative Biology, Massachusetts General Hospital and Harvard Medical School, Boston, MA 02114, USA
[5]Gastrointestinal Unit, Center for the Study of Inflammatory Bowel Disease, Massachusetts General Hospital and Harvard Medical School, Boston, MA 02114, USA
[6]Department of Veterinary Medicine, University of Cambridge, Madingley Road, Cambridge CB23 8AQ, UK
[7]Cancer Metabolism Research Unit, Cancer Research UK, Beatson Institute, Garscube Estate, Switchback Road, Bearsden, Glasgow G61 1BD, UK
[8]Department of Microbiology, Moyne Institute for Preventative Medicine, School of Genetics and Microbiology, Trinity College Dublin, Dublin 2, Ireland
[9]Institute of Biotechnology, 00014 University of Helsinki, P.O. Box 56, Helsinki 00014, Finland
[10]BioMediTech and Tampere University Hospital, University of Tampere, Tampere 33014, Finland
[11]Max-Planck-Institute for Heart and Lung Research, Ludwigstrasse 43, 61231 Bad Nauheim, Germany
[12]Co-first author
[13]Present address: GlaxoSmithKline, Gunnels Wood Road, Stevenage, Hertfordshire SG1 2NY, UK
[14]Lead Contact
*Correspondence: mpm@mrc-mbu.cam.ac.uk (M.P.M.), laoneill@tcd.ie (L.A.O.)
http://dx.doi.org/10.1016/j.cell.2016.08.064

SUMMARY

Activated macrophages undergo metabolic reprogramming, which drives their pro-inflammatory phenotype, but the mechanistic basis for this remains obscure. Here, we demonstrate that upon lipopolysaccharide (LPS) stimulation, macrophages shift from producing ATP by oxidative phosphorylation to glycolysis while also increasing succinate levels. We show that increased mitochondrial oxidation of succinate via succinate dehydrogenase (SDH) and an elevation of mitochondrial membrane potential combine to drive mitochondrial reactive oxygen species (ROS) production. RNA sequencing reveals that this combination induces a pro-inflammatory gene expression profile, while an inhibitor of succinate oxidation, dimethyl malonate (DMM), promotes an anti-inflammatory outcome. Blocking ROS production with rotenone by uncoupling mitochondria or by expressing the alternative oxidase (AOX) inhibits this inflammatory phenotype, with AOX protecting mice from LPS lethality. The metabolic alterations that occur upon activation of macrophages therefore repurpose mitochondria from ATP synthesis to ROS production in order to promote a pro-inflammatory state.

INTRODUCTION

Macrophages have two key roles: to respond rapidly to infection and injury and then to help repair the tissue damage that occurs as a result of this response. This requires macrophages to initially adopt a pro-inflammatory phenotype and then later, when the immediate danger has passed, to acquire an anti-inflammatory phenotype to promote resolution and repair. The factors that drive and sustain these changes are not fully understood. However, multiple lines of evidence implicate alterations in mitochondrial function, reactive oxygen species (ROS) production, and related metabolic pathways in this phenotypic switch (O'Neill and Pearce, 2016). For example, pro-inflammatory macrophages are more glycolytic, produce more ROS, and accumulate succinate to a greater extent than resting macrophages (O'Neill and Pearce, 2016). Even so, the mechanisms and significance of these changes are obscure. The electron transport chain (ETC) is a major component of mitochondrial metabolism, and resting macrophages utilize this efficient form of oxidative metabolism to generate ATP. However, once macrophages are activated (e.g., with the Toll-like receptor 4 [TLR4] agonist lipopolysaccharide [LPS]), oxidative phosphorylation is suppressed, and cells favor glycolysis as an alternative, but less energetically efficient, mode of ATP generation (Tannahill et al., 2013). In dendritic cells (DCs), the switch to glycolysis and away from oxidative phosphorylation supports fatty acid synthesis required for the expansion of organelles necessary

for the production and secretion of key proteins essential for DC activation (Everts et al., 2014) and to prevent apoptosis in the face of a lowered level of ATP production by oxidative phosphorylation (Everts et al., 2012). TLR4 stimulation will also lead to mitochondrial ROS generation from complex I through an unknown mechanism (West et al., 2011). On the other hand, activated T cells maintain oxidative phosphorylation in conjunction with glycolysis, but whether oxidative metabolism is required for the production of biosynthetic precursors and ATP following stimulation or to generate a ROS signal is unclear (Sena et al., 2013). Here, we set out to determine the mechanistic rationale underlying the mitochondrial, ROS, and metabolic changes in macrophages that determine the inflammatory status of the cell, noting that all are linked by electron transfer in the ETC. We have found that following stimulation with LPS, macrophages repurpose their mitochondria from ATP production to succinate-dependent ROS generation, with glycolysis taking on the role of ATP generation, enabling mitochondria to sustain a high membrane potential. Thus, the enhanced production of succinate is a critical regulator of the pro-inflammatory response to LPS, both through the generation of ROS following oxidation by the ETC and via HIF-1α stabilization. Concurrently, anti-inflammatory gene expression is decreased following succinate oxidation. These events demonstrate a role for succinate oxidation by the ETC in the pro-inflammatory response to LPS and provide insights into the previously elusive mechanism by which macrophages generate mitochondrial ROS. We have identified a process whereby mitochondrial metabolism is intimately linked to the profound gene expression changes that occur in macrophages in order for them to fulfill their dual role in inflammation and its resolution.

RESULTS

Succinate Drives IL-1β Production and Limits the Production of IL-1RA and IL-10

Succinate is a well established pro-inflammatory metabolite that is known to accumulate during macrophage activation, the levels of which affect HIF-1α activity, a key transcription factor in the expression of pro-inflammatory genes (Tannahill et al., 2013). We therefore examined the effects of pretreatment of LPS-activated bone-marrow-derived macrophages (BMDMs) with cell-permeable diethyl succinate (hereafter referred to as succinate), which greatly increases succinate in the cytosol and mitochondrial matrix. Succinate enhanced LPS-induced interleukin-1β (IL-1β) mRNA and pro-IL-1β protein with an accompanying boost in HIF-1α protein levels (Figures 1A–1C), as previously shown (Tannahill et al., 2013). Succinate also boosted LPS-induced glycolysis (Figure S2A). Importantly, this synergistic effect of exogenous succinate and LPS did not occur for another pro-inflammatory cytokine, tumor necrosis factor-α (TNF-α) (Figures 1D and 1E), demonstrating the specificity of this response. Succinate alone had no effect on cytokine production, nor did it affect LPS-induced nuclear factor κB (NF-κB) activation either on its own (Figure 1F, left) or in combination with LPS (Figure 1F, right), as measured by p65 phosphorylation (Figure 1F, top) or IκB degradation (Figure 1F, third panel). Conversely, succinate inhibited the induction of the anti-inflammatory cytokines IL-1RA (Figure 1G) and IL-10 (Figure 1H) in response to LPS. The effect of succinate on IL-10 was rapid, being evident from 1 hr, and sustained for both mRNA (Figure 1H) and protein (Figure 1I) induction, and it was concentration dependent (Figure 1J). While two other Krebs cycle metabolites, α-ketoglutarate (α-KG) and fumarate, increased the LPS-induced IL-1β message, their effects on LPS-induced pro-IL-1β were far less robust than for succinate (Figures S1A and S1B), and only succinate decreased LPS-induced IL-10 production (Figure S1C, left). Furthermore, fumarate also boosted LPS-induced TNF-α, suggesting its pro-inflammatory effects are mechanistically distinct from succinate (Figure S1C, right). Moreover, diethyl butyl malonate (DEBM), an inhibitor of the mitochondrial succinate transporter, which causes endogenous succinate to accumulate, boosted LPS-induced IL-1β and limited IL-10, with no effect on TNF-α (Figures S1D–S1F). These findings suggest that succinate acts within the cell to enhance and sustain endogenous pro-inflammatory gene expression while at the same time inhibiting anti-inflammatory gene expression.

Mitochondrial Succinate Oxidation Alters the Expression of Pro- and Anti-inflammatory Genes

To examine how succinate within macrophages might have opposing effects on pro- and anti-inflammatory pathways, we investigated two of the ways in which succinate could act within the cell, either by enhancing HIF-1α activation by inhibiting prolyl hydroxylase (PHD) function or as a result of oxidation by mitochondrial succinate dehydrogenase (SDH). Succinate was found to robustly boost LPS-induced HIF-1α protein levels, an effect that was not observed by any other metabolite tested (Figure S2D). Moreover, the HIF-1α activator dimethyloxalylglycine (DMOG) mimicked the effect of succinate on IL-1β (Figures S2F, right, and S2G). Succinate did not alter the expression of cMyc, another transcription factor with a known role in the regulation of macrophage function (Pello et al., 2012), nor did it alter the expression of its downstream target, CD71 (Figures S2H–S2J). We therefore conclude that succinate's pro-inflammatory effects require HIF-1α stabilization.

We also tested the cell-permeable molecule dimethyl malonate (DMM), which is rapidly hydrolyzed within the cell to generate malonate, a potent competitive inhibitor of succinate oxidation by SDH (Dervartanian and Veeger, 1964). DMM led to an increase in succinate in the cytosol, presumably by impairing the oxidation of succinate to fumarate, and also boosted LPS-induced succinate accumulation (Figure 2A). Importantly, succinate and malonate were the only two metabolites significantly altered by the addition of DMM in the presence or absence of LPS, demonstrating specificity (Figures S3A–S3J). DMM should inhibit effects of succinate that act through SDH in the mitochondria but enhance succinate action through PHD in the cytosol (as a result of the succinate boost evident by this agent). Intriguingly, in direct opposition to succinate, DMM abrogated LPS-induced IL-1β mRNA (Figure 2B), pro-IL-1β protein, and HIF-1α (Figure 2C, compare lane 5 to lane 7) while leaving TNF-α unaffected (Figures 2D and 2E). The primers used for the PCR are described in Table S7. At earlier time points, it appeared that DMM limited LPS-induced cMyc (Figure S2H); however, this was not significant, and at later time points, when DMM alters IL-1β, DMM

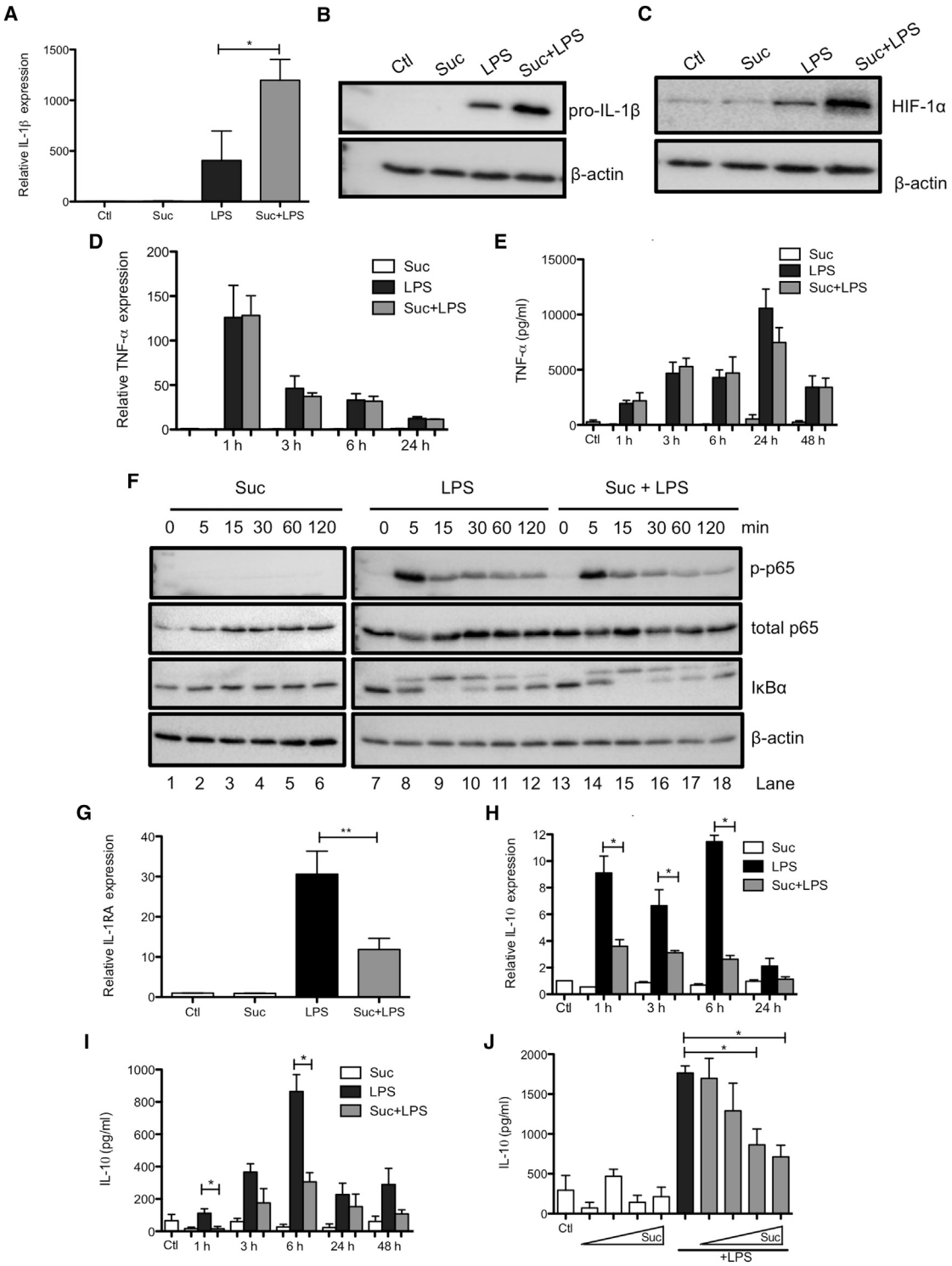

Figure 1. Succinate Drives IL-1β Production and Limits the Production of IL-1RA and IL-10

(A–J) BMDMs were pretreated for 3 hr with succinate (Suc; 5 mM; A–I; or 0.2–5 mM, J) before being stimulated with LPS (100 ng/mL) for 48 hr (A–C, G, and J) or the indicated times (D–F, H, and I). mRNA was extracted from total cell lysates and analyzed by qPCR for IL-1β (A), TNF-α (D), IL-1RA (G), and IL-10 (H) expression. Whole-cell lysates were analyzed by western blotting for pro-IL-1β, HIF-1α, phospho-p65, total p65, IκBα, and β-actin (B, C, and F). Supernatants were analyzed by ELISA for TNF-α (E) and IL-10 production (I and J). The data in (A), (D), (E), and (G–J) represent mean ± SEM, n = 3; *$p < 0.05$, **$p < 0.01$. The blots in (B), (C), and (F) are representative of three independent experiments.

See also Figures S1 and S2.

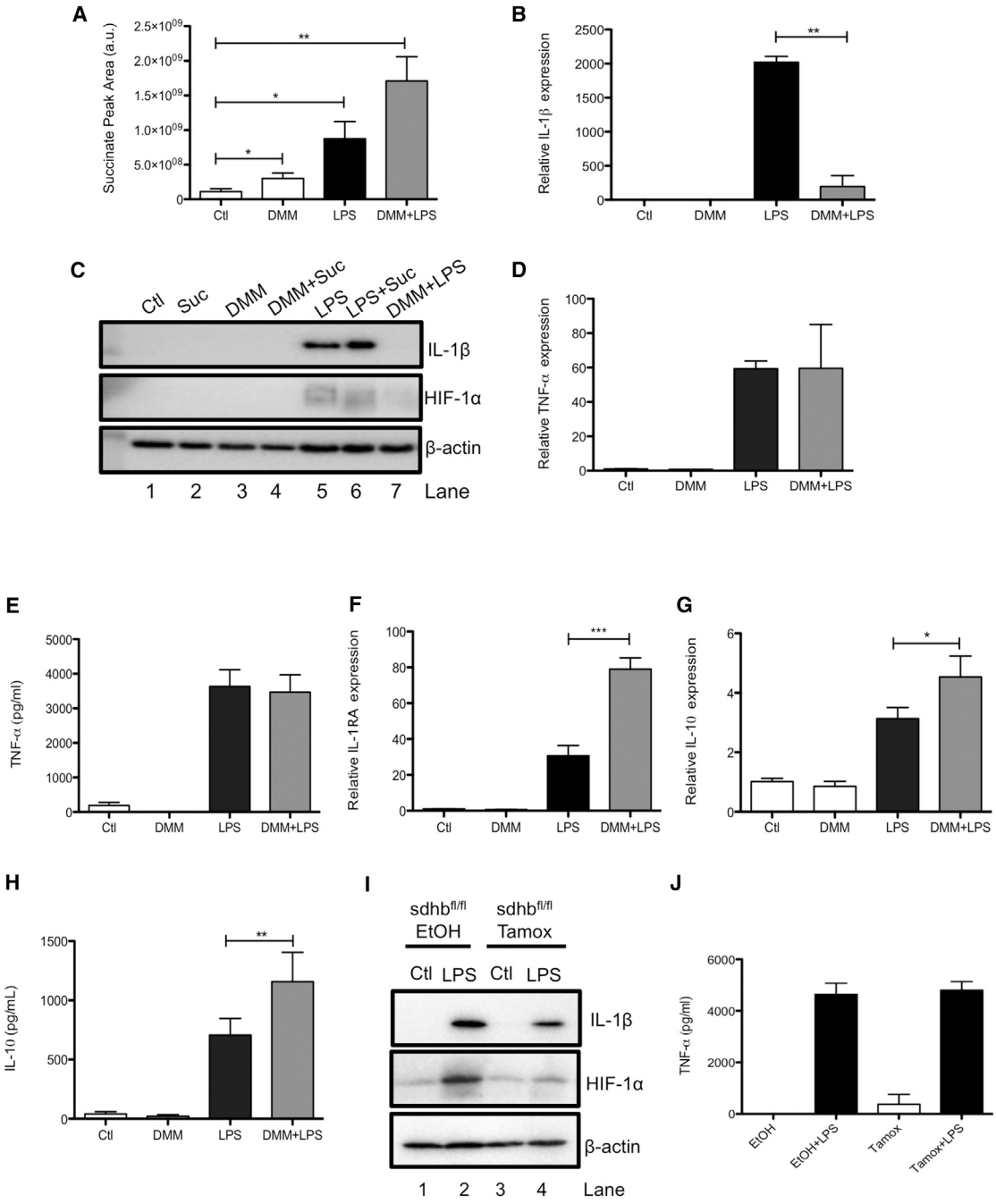

Figure 2. Inhibition of Succinate Dehydrogenase Impairs LPS-Induced IL-1β Production and Boosts IL-1RA and IL-10

(A–J) BMDMs were pretreated for 3 hr with dimethyl malonate (DMM; 10 mM) prior to stimulation with LPS (100 ng/mL) for 24 hr (A), 48 hr (B, C, E, G, and H), or 4 hr (D and F). SDHB-proficient (SDHB$^{fl/fl}$ EtOH) and SDHB-deficient (SDHB$^{fl/fl}$ Tamox) BMDMs were untreated (Ctl) or treated with LPS (100 ng/μL) for 24 hr (I and J). Lysed cells were analyzed by liquid chromatography-mass spectrometry (LC-MS) to determine succinate levels (A). mRNA from total cell lysates was analyzed by qPCR for IL-1β (B), TNF-α (D), IL-1RA (F), and IL-10 (G) expression. Whole-cell lysates were analyzed by western blotting for pro-IL-1β, HIF-1α, and β-actin (C and I). Supernatants were analyzed by ELISA for TNF-α (E and J) and IL-10 production (H). The data in (A), (B), and (D–H) represent mean ± SEM, n = 3. The data in (J) represent mean ± SEM, n = 6; *$p < 0.05$, **$p < 0.01$, ***$p < 0.001$. The blots are representative of three (C) or five (J) independent experiments.
See also Figures S1 and S3.

had no effect on cMyc (Figures S2I and S2J). Again, in opposition to succinate, DMM boosted LPS-induced IL-1RA (Figure 2F) and IL-10 expression and production (Figures 2G and 2H). These data indicate that, in addition to direct effects on PHDs in the cytosol, the oxidation of succinate by mitochondria is central to the pro-inflammatory response of LPS-activated macrophages.

As IL-10 and IL-1β were reciprocally regulated by DMM, we examined whether IL-10 itself may be responsible for the regulation of IL-1β by this compound. This was not the case, as DMM still inhibited LPS-induced pro-IL-1β in the presence of an IL-10 receptor blocking antibody (Figure S2K).

To further examine a role for SDH activity in the pro-inflammatory effects of succinate, we next employed macrophages from mice lacking the B subunit of SDH. The B subunit is required for succinate to reduce ubiquinone (Guzy et al., 2008), and its absence will therefore block succinate oxidation. LPS-induced pro-IL-1β and HIF-1α were decreased in SDHB-deficient BMDMs (Figure 2I, top and middle, respectively; compare lane 2 to lane 4), while TNF-α was unchanged (Figure 2J).

To gain further insight into how the manipulation of mitochondrial succinate oxidation might alter the phenotype of macrophages, we next determined the effects of succinate and DMM on the macrophage genome by performing RNA-sequencing analysis. This revealed whole sets of LPS-induced genes that were altered by DMM or succinate pretreatment (Figures 3 and S3K–S3M; Tables S1, S2, S3, S4, S5, and S6). The gene expression values in different samples were modeled with a generalized linear model (detailed in STAR Methods). Of particular relevance is that many genes that were downregulated by DMM were reciprocally upregulated by succinate and vice versa (Figure S3M), further suggesting that the metabolism of succinate by SDH is crucial for its pro-inflammatory action. These gene sets were related to immune response pathways, including interferon (IFN) signaling, the cellular response to hypoxia, fatty acid metabolism, glycolytic processes, and positive and negative regulation of homeostasis (illustrated in Figure 3B). A direct comparison of LPS stimulation under pretreatment with DMM or succinate confirmed this, as several biological pathways related to homeostasis, metabolism, and inflammation were affected (Figure 3C), even under this stricter comparison. Most importantly, DMM suppressed expression of genes associated with inflammation (including those encoding IL-1β, HIF-1α-dependent genes, and genes involved in fatty acid synthesis) while boosting anti-inflammatory gene expression (such as the gene encoding IL-1RA and several type I IFN-inducible genes) (Figure 3B, blue histobars). Succinate had the opposite effect, boosting pro-inflammatory gene expression while decreasing anti-inflammatory gene expression (Figure 3B, red histobars). The reciprocal regulation of IL-1β and IL-1RA (both indicated with an arrow) is especially noteworthy. Type I IFNs are also of interest, as they inhibit LPS-induced pro-IL-1β production and boost IL-10 in BMDMs (Guarda et al., 2011), providing further mechanistic evidence for the regulation of IL-10, and indeed of IL-1β, by these agents. As expected, RNA sequencing revealed that succinate induced, while DMM limited, HIF-1α activity. These findings suggest that HIF-1α is an important part of the mechanism by which succinate and DMM regulate IL-1β and confirm that the extent of succinate oxidation by mitochondrial SDH controls LPS-induced gene expression. When active, SDH boosts inflammatory gene expression, and when inhibited, an anti-inflammatory phenotype ensues.

Taken together, these results indicate that SDH is a critical regulator of the macrophage phenotype. Inhibiting SDH causes succinate to accumulate but importantly prevents the induction of a range of pro-inflammatory factors, typified by IL-1β, while enhancing a range of anti-inflammatory factors, typified by IL-1RA and IL-10. Increased oxidation of succinate by SDH in mitochondria is therefore required for the induction of pro-inflammatory genes while simultaneously limiting the induction of anti-inflammatory ones.

Inhibition of Succinate Dehydrogenase In Vivo Is Anti-inflammatory

To examine if SDH activity was also involved in the pro-inflammatory response in vivo, we next investigated the effect of DMM on LPS action in mice. DMM was effective in an LPS-induced sepsis model, where it decreased serum levels of IL-1β (Figure 4A) and boosted IL-10 (Figure 4B), but had no significant effect on TNF-α (Figure 4C). DMM reduced IL-1β (Figures 4D and 4E) and PHD3 expression (Figure 4F) in the spleen. SDH activity is therefore critical for determining the inflammatory phenotype, both in vitro and in vivo.

Glycolytic ATP Production Facilitates an Increase in Mitochondrial Membrane Potential that Is Required for the Pro-inflammatory Effects of LPS

To further explore the mechanism by which SDH might affect the macrophage phenotype, we next considered how SDH activity interacts with other metabolic changes occurring in LPS-activated macrophages. A hallmark of the pro-inflammatory phenotype of macrophages is their switch away from ATP production by oxidative phosphorylation to glycolytic metabolism (O'Neill and Pearce, 2016; Tannahill et al., 2013). Previous work showed that inhibiting glycolysis with 2-deoxyglucose (2DG) prevented activation of HIF-1α and induction of IL-1β in LPS-treated macrophages yet had no effect on TNF-α production (Tannahill et al., 2013) (Figures S4A–S4D). These data suggested that the enhanced glycolytic ATP production upon activation may act in combination with the stimulation of SDH to sustain the pro-inflammatory phenotype. We hypothesized that the increased ATP generated by glycolysis in the cytosol would significantly decrease the requirement for mitochondrial oxidative phosphorylation to supply ATP to the cell. Such a shift would decrease resting oxygen consumption by the mitochondrial respiratory chain, as has been shown previously (Tannahill et al., 2013). Here, we demonstrate that glycolysis is boosted by LPS (Figure 5A) and oxygen consumption is decreased (Figure 5B), yet not abrogated, by LPS (Figure 5E). LPS decreased the ATP/ADP ratio consistent with a shift from ATP synthesis by oxidative phosphorylation to ATP synthesis by glycolysis (Figure 5D). Importantly, addition of oligomycin, which will abolish any contribution to ATP synthesis by the ETC, to control cells dramatically decreased respiration yet had no effect on the ATP/ADP ratio in LPS-treated cells (Figure 5D). Taken together, these data indicate that following LPS treatment, cells were not making ATP by mitochondrial oxidative phosphorylation. It is interesting to note that inhibition of the ATP synthase with oligomycin decreased LPS-induced IL-1β, suggesting that some level of ATP synthesis within the mitochondrial matrix may be necessary for the generation of a pro-inflammatory response (Figure S5). The NAD^+/NADH ratio also decreased with LPS treatment (Figure 5C), consistent with a decrease in mitochondrial NADH oxidation and complex I forward activity.

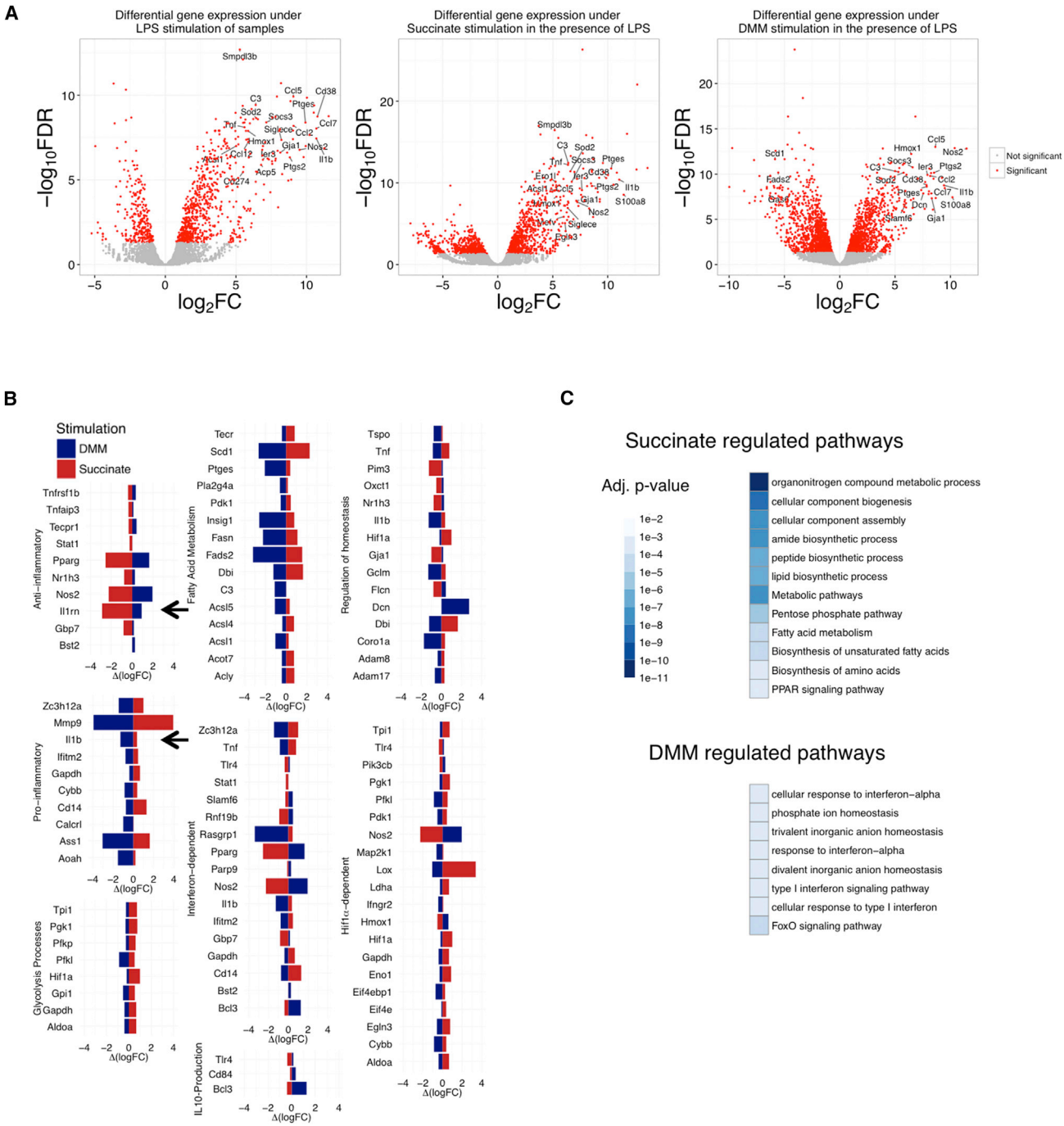

Figure 3. Limiting Succinate Oxidation Induces an Anti-inflammatory Response

BMDMs were pretreated with dimethyl malonate (DMM; 10 mM) or succinate (5 mM) for 3 hr before being stimulated with LPS (100 ng/μL) for 4 or 48 hr. RNA was isolated, and RNA sequencing was performed. Gene expression in the different stimulations and time points was modeled with a generalized linear model, and fold changes and false discovery rate (FDR)-adjusted p values were calculated.

(A) Distribution of the fold changes (log_2FC) and the FDR-adjusted p values (log FDR) for the comparison between LPS-treated samples and control without and with pretreatment with succinate and DMM. A large number of genes were found to be oppositely regulated when pretreated with succinate as compared to when they were pretreated with DMM. Significant changes are colored red, while the insignificant changes are colored gray.

(B) Difference in fold changes when the BMDMs were pretreated with either DMM or succinate as compared to when they were not. The genes are annotated for the immune pathways they belong to.

(legend continued on next page)

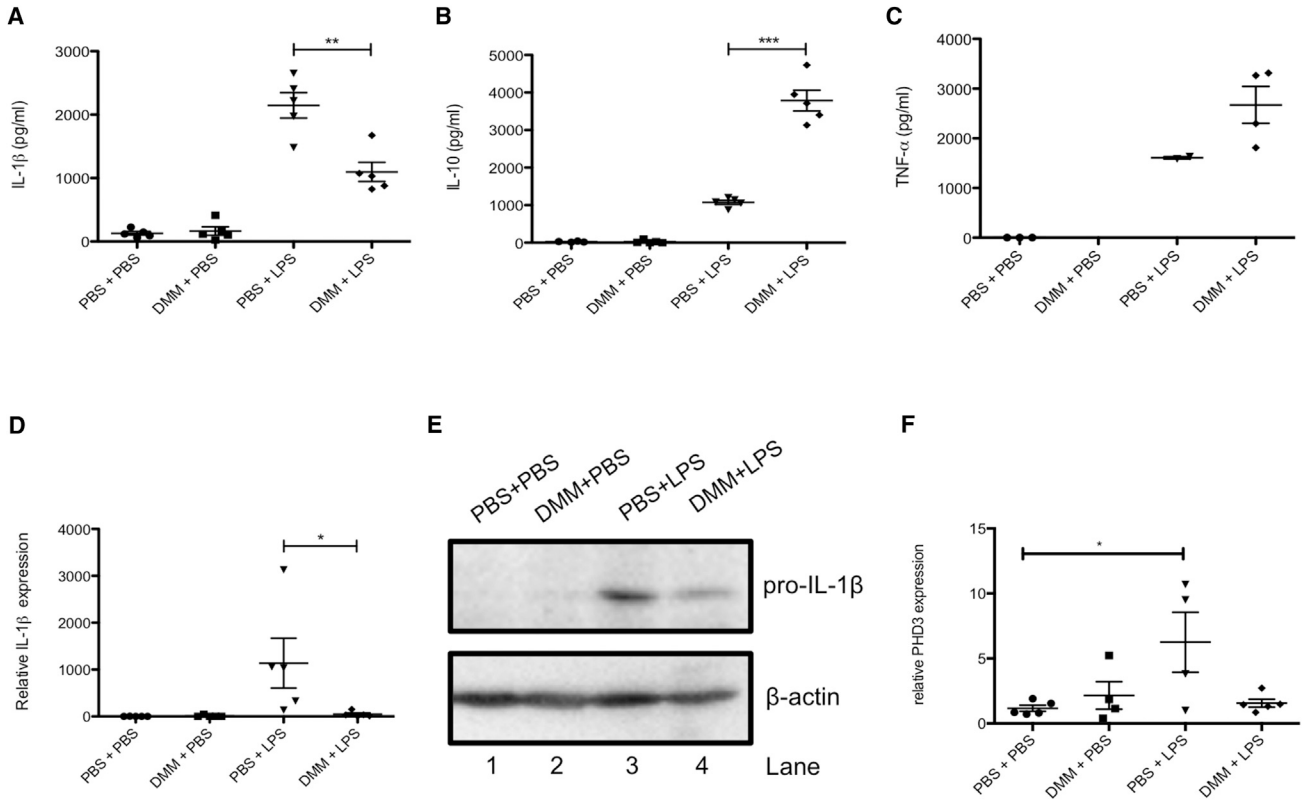

Figure 4. Inhibition of Succinate Dehydrogenase In Vivo Is Anti-inflammatory

Mice were injected intraperitoneally (i.p.) with DMM (160 mg/kg) or PBS for 3 hr, followed by PBS or LPS (15 mg/kg) for 2 hr.

(A–C) Serum was isolated from whole blood, and IL-1β (A), IL-10 (B), and TNF-α (C) production were measured by ELISA.

(D–F) Spleens were isolated, IL-1β (D) and PHD3 (F) expression was analyzed by qPCR, and pro-IL-1β and β-actin were measured by western blotting (E).

The data in (A)–(D) and (F) represent mean ± SEM, n = 5 per group; *p < 0.05, **p < 0.01, ***p < 0.001. Blots are representative of one sample from each treatment group.

Cells that are making ATP by glycolysis and not by mitochondrial oxidative phosphorylation, as in the case of LPS activation, are expected to have a higher mitochondrial membrane potential ($\Delta\Psi_m$). This is because the $\Delta\Psi_m$, which is generated by proton pumping through complexes I, III, and IV across the mitochondrial inner membrane, is no longer being used by the ATP synthase to make ATP. We found that LPS increased $\Delta\Psi_m$ as measured by potential-sensitive tetramethylrhodamine methyl ester (TMRM) fluorescence using flow cytometry and confocal microscopy (Figures 5F–5H). The percentage of cells with an elevated $\Delta\Psi_m$ increased from 6.18% to 47.1% in response to LPS, and this was decreased to 26.1% when glycolysis was inhibited with 2DG (Figure 5I). This suggests that the increased ATP supply by glycolysis and the consequential decrease in requirement for mitochondrial ATP production leads to an increase in the $\Delta\Psi_m$ that is important for LPS signaling. To determine if there was indeed a requirement for increased membrane potential in LPS signaling, we next explored the effect of the uncoupler carbonylcyanide m-chlorophenylhydrazone (CCCP) on LPS-activated macrophages. As expected, the addition of CCCP led to a decrease in $\Delta\Psi_m$ (Figure 5H) and a boost in respiration, which reached its maximum effect on these variables at 5-10 μM CCCP indicating complete uncoupling (Figure S4G). Concentrations of CCCP sufficient to uncouple mitochondria also decreased LPS-induced IL-1β expression (Figures 5J and S4H) and pro-IL-1β levels (Figure 5K, compare lane 7 to lanes 8–10) but only affected TNF-α at higher concentrations where cellular viability was impaired (Figures S4F and S4J). Dissipation of the mitochondrial membrane potential with CCCP or 2DG also impaired LPS-induced IL-10 production (Figure 5M and 5N, respectively), suggesting that coupled mitochondria are required for the production of this anti-inflammatory cytokine. Importantly, the lack of effect by both CCCP and 2DG on TNF-α (Figures 5L and S4D, respectively) demonstrates that this

(C) Results of functional enrichment of our gene expression analysis in the KEGG (Kyoto Encyclopedia of Genes and Genomes) and Reactome pathway databases. The heatmap represents the statistical significance (FDR-adjusted p value) of the different pathways found to be enriched in our analysis, with the darker colors denoting pathways enriched with higher confidence.

See also Figure S3 and Tables S1–S6.

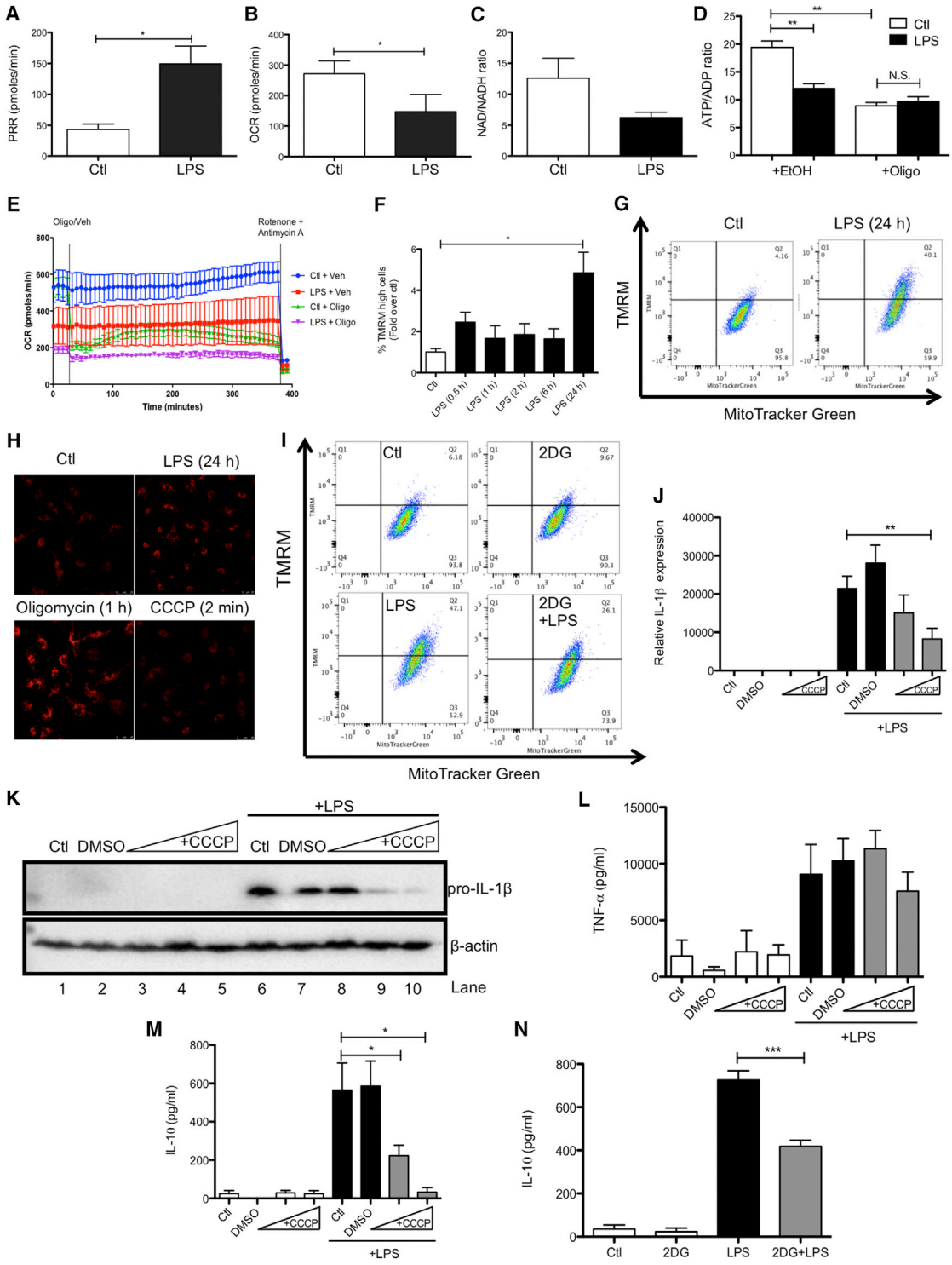

Figure 5. Glycolytic ATP Production Facilitates an Increase in Mitochondrial Membrane Potential that Is Required for the Pro-inflammatory Effects of LPS

(A–E) BMDMs were stimulated with LPS (100 ng/mL) for 48 hr (A and B) or 24 hr (C and D). The oxygen consumption rate (OCR) and proton production rate (PPR) were analyzed as readouts for oxidative phosphorylation and glycolysis, respectively, using the Seahorse XF-24. The NAD^+/NADH ratio in cell lysates was determined using an NAD^+/NADH assay kit (C). The ATP/ADP ratio in cell lysates was determined using an ATP/ADP assay kit (D). BMDMs were untreated (Ctl) or stimulated with LPS (100 ng/mL) for 24 hr before OCR analysis using the Seahorse XF-24 (E). During the Seahorse run, BMDMs were first injected with oligomycin

(legend continued on next page)

cytokine is regulated differently than IL-1β or IL-10, most likely by a mitochondria-independent mechanism. Together, these data suggest that the shift from oxidative phosphorylation to glycolysis and the consequent elevation in $\Delta\Psi_m$, in conjunction with the increased succinate, together provide a pro-inflammatory signal.

Increased Membrane Potential and Succinate Oxidation Induce the Generation of Mitochondrial ROS that Drives IL-1β

As mitochondrial ROS production is greatly enhanced by both an increase in $\Delta\Psi_m$ and an increase in SDH activity (Chouchani et al., 2016), we next examined whether ROS could act as a redox signal emanating from mitochondria to drive IL-1β production. Addition of LPS led to an increase in ROS as measured by both MitoSOX and CellROX (Figures S6A and 6A). DMM limited LPS-induced ROS (Figures 6A and S6D), while succinate boosted ROS production (Figures 6C and S6B). This ROS signal led to increased IL-1β expression as evidenced by the use of a variety of ROS scavengers. The mitochondria-targeted antioxidants MitoQ (Kelso et al., 2001) (Figure 6B, left; compare lanes 3 and 4 to lanes 7 and 8) and MitoTEMPO (Figure 6B, right; compare lanes 3 and 4 to lanes 7 and 8 and lanes 11 and 12) and the thiol reductant N-acetylcysteine (Figure S6C; compare lanes 3 and 4 to lanes 7 and 8 and lanes 11 and 12) all inhibited the effect of succinate on LPS-induced pro-IL-1β and HIF-1α, suggesting that this ROS signal was critical for IL-1β production in response to succinate. In addition, LPS-induced ROS production was prevented by dissipating the mitochondrial membrane potential with CCCP (Figures 6D and S6E). Together, these data suggest that increased succinate oxidation and an elevation of the mitochondrial membrane potential are both required to generate a pro-inflammatory mitochondrial ROS signal.

The complex I inhibitor rotenone significantly decreased LPS-induced ROS (Figures 6E and S6F) while also decreasing LPS-induced IL-1β mRNA expression (Figure 6F) and pro-IL-1β (Figure 6G, compare lane 7 to lanes 8–10) yet had no effect on TNF-α (Figure 6H), supporting a role for complex I activity in ROS production in this system. To further investigate the role of mitochondrial ROS in LPS-activated macrophages, we used BMDMs from mice expressing an alternative oxidase (AOX) from *Ciona intestinalis* (El-Khoury et al., 2014) AOX provides a pathway to oxidize excess electrons that build up in the ubiquinone (CoQ) pool (as a result of succinate accumulation, for example) that can contribute to mitochondrial ROS production. AOX was confirmed to be present in BMDMs from these mice (Figure 6I) (Fernandez-Ayala et al., 2009). AOX expression in BMDMs impaired the boost in ROS production following LPS treatment (Figures 6J and S4K) and strongly impaired the boost in LPS-induced IL-1β and HIF-1α with succinate (Figure 6M, compare lanes 3 and 4 to lanes 7 and 8). There was no difference in the observed LPS-induced boost in membrane potential between wild-type and AOX-expressing BMDMs (Figures 4K and 4L). Crucially, AOX expression increased the survival of mice injected with LPS. There was 50% mortality in wild-type mice, while survival remained above 80% in AOX-expressing mice (Figure 6N). These data suggest that limiting ROS production either pharmacologically or using genetic approaches limits IL-1β levels and is protective against LPS lethality, supporting a role for mitochondrial ROS production in inflammation.

DISCUSSION

Alterations in mitochondrial metabolism following LPS treatment of macrophages are now understood to be vital for an appropriate immune response (Mills and O'Neill, 2016). Studies dating back to the 1970s demonstrated that LPS attenuates macrophage respiration by inhibiting complexes II and III (Kato, 1972) and slowing state III respiration (McGivney and Bradley, 1979). LPS also alters the Krebs cycle, effectively breaking it at two points: after citrate and after succinate (Jha et al., 2015). Furthermore, previous studies have shown that LPS increases mitochondrial ROS production (West et al., 2011) as an important response for bacterial killing in macrophages, but the mechanism was obscure. Our study shows that mitochondrial ROS generation following the oxidation of succinate is central to determining the inflammatory phenotype of macrophages.

This study provides a model that explains the many disparate aspects of the metabolic changes that occur upon activation of macrophages with LPS. Together, these findings suggest that an important consequence of the shift to glycolytic ATP production upon activation of macrophages is the release of mitochondria from their requirement to produce ATP by oxidative phosphorylation, thereby enabling the mitochondrial membrane

(Oligo; 10 μM) or vehicle (EtOH), and OCR was measured for the following 6 hr. At this point, rotenone (Rot; 100 nM) and antimycin A (4 μM) were injected to all wells to abolish OCR.

(F–I) BMDMs were untreated (Ctl), treated with LPS (100 ng/mL) for the indicated times (F and G), or pretreated with 2-deoxyglucose (2DG; 1 mM) for 3 hr prior to LPS for 24 hr (I). Cells were costained with TMRM (20 nM) and MitoTracker Green (50 nM) for 30 min and then analyzed by fluorescence-activated cell sorting (FACS) to quantify the membrane potential. The intensity of TMRM staining reflects the membrane potential. To analyze the membrane potential by confocal microscopy, BMDMs were untreated (Ctl), treated with LPS (100 ng/mL) for 24 hr, oligomycin (Oligo: 5 μM) for 1 hr or with carbonylcyanide m-chlorophenylhydrazone (CCCP; 10 μM) for 2 min (H). Cells were stained with TMRM (20 nM) for 30 min prior to imaging. The intensity of TMRM staining reflects the membrane potential.

(J–N) BMDMs were also pretreated with CCCP (0.5-10 μM; J–M), or 2DG (1 mM; N) for 3 hr before being stimulated with LPS (100 ng/mL) for 4 hr (J–M) or 48 hr (N). mRNA was extracted from total cell lysates and analyzed by qPCR for IL-1β expression (J), and whole-cell lysates were analyzed by western blotting for pro-IL-1β and β-actin (K). Supernatants were analyzed by ELISA for TNF-α (L) and IL-10 (M and N) production.

The data in (A)–(D) and (J)–(M) represent mean ± SEM, n = 3; *p = 0.05, **p < 0.01, ***p < 0.001. The data in (F) shows quantification of TMRM high cells and represents mean ± SEM; *p < 0.05. The cytometric dot plots in (G) and (I) are representative of three (G) or four (I) separate experiments. Images in (H) are representative of five separate experiments. The blots in (K) are representative of three independent experiments. The Seahorse OCR data in (E) are representative of four independent experiments.

See also Figures S4 and S5.

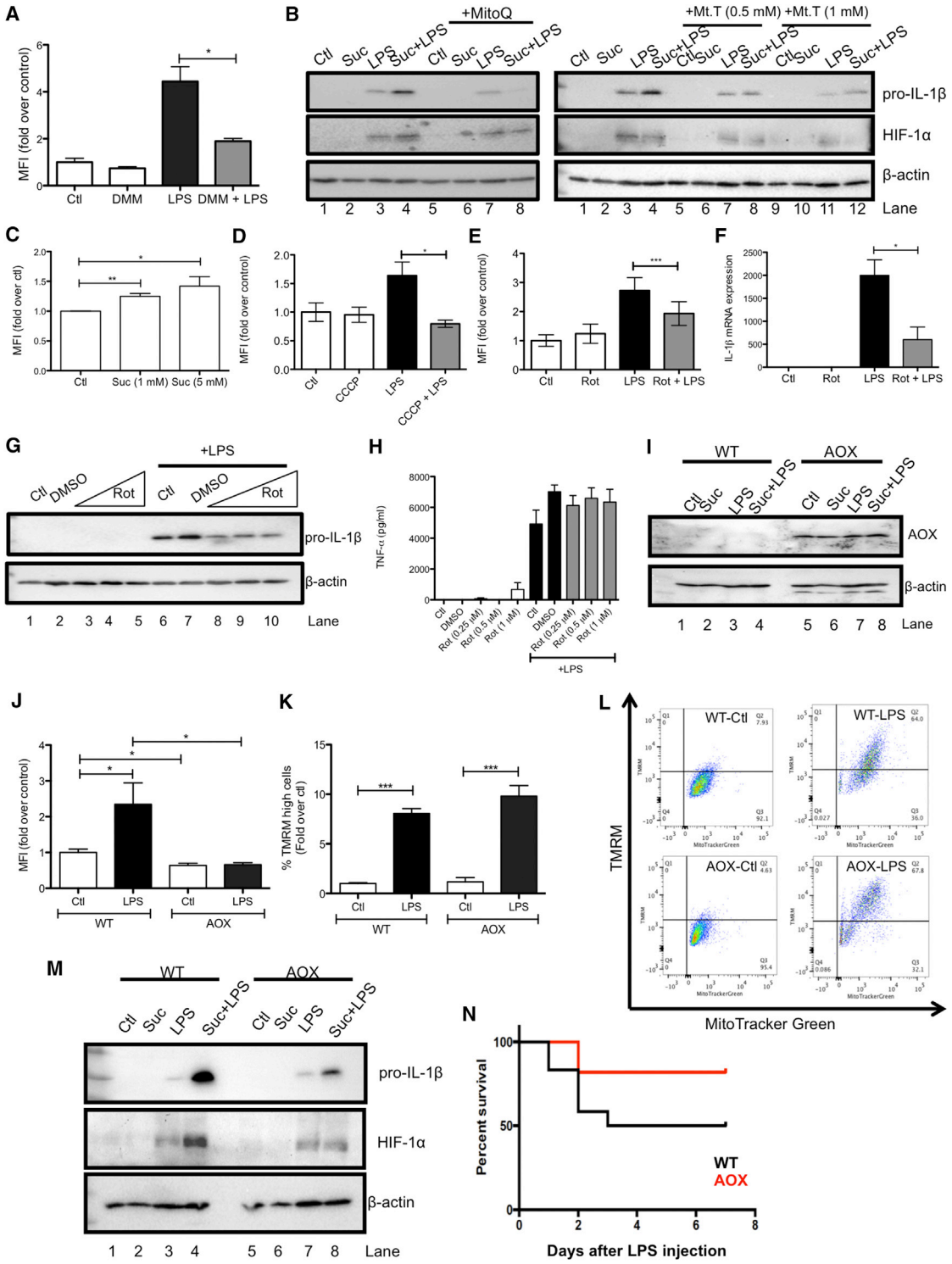

Figure 6. Inhibition of ROS Production by Impairing Complex I or II Activity or by Dissipating the Membrane Potential Limits IL-1β Production in LPS-Activated Macrophages

(A–G) BMDMs were pretreated for 3 hr with dimethyl malonate (DMM; 10 mM; A), carbonylcyanide m-chlorophenylhydrazone (CCCP; 7.5 μM; D), or rotenone (Rot; 0.5 μM; E) before being stimulated with LPS (1 μg/mL; A, E, and F) for 24 hr (A, E, and F) or 4 hr (D) or were treated with succinate (Suc; 1–5 mM) for 24 hr (C). Live cells were analyzed by FACS, and mean fluorescence intensity (MFI) was quantified as a measure of cellular reactive oxygen species production. BMDMs were pretreated with MitoQ (500 nM) or MitoTEMPO (Mt.T; 0.5–1 mM) for 1 hr prior to the addition of succinate (Suc; 5 mM) for 3 hr before stimulation with LPS (100 ng/mL) for 48 hr (B). BMDMS were also pretreated for 3 hr with rotenone (Rot; 0.1–1 μM; F and G) prior to stimulation with LPS (100 ng/ml) for 24 hr.

(legend continued on next page)

potential to increase. This is coupled with the remodeling of metabolism to funnel metabolites to succinate, the oxidation of which we have demonstrated is critical in the regulation of the inflammatory state of macrophages. We demonstrate that succinate oxidation and a high mitochondrial membrane potential generate a redox signal that can alter HIF-1α activity. This is in agreement with a recent study performed in keratinocytes demonstrating a critical role for ROS derived from the ETC in HIF-1α stabilization (Hamanaka et al., 2016). Crucially, we report that these events alter the expression levels of a range of pro- and anti-inflammatory genes. The inflammatory phenotype of the macrophage, as indicated by increased inflammatory gene expression and reciprocally decreased anti-inflammatory gene expression, is governed by succinate oxidation by SDH. We demonstrate that ROS drive expression of cytokines such as IL-1β via HIF-1α. Precisely how succinate inhibits anti-inflammatory gene expression is under investigation. This may involve succinate-induced regulation of other members of the α-KG-dependent dioxygenase family, such as those involved in epigenetic changes occurring in macrophages (Yang and Pollard, 2013). We are currently investigating this possibility. From our data, it is clear, nevertheless, that SDH is a key arbiter of the inflammatory response in macrophages. Furthermore, our observation that TNF-α is not controlled by SDH points to specificity in the role of the mitochondria in the regulation of cytokine production. In a recent study by Sancho and colleagues, live bacteria were shown to alter the assembly of the ETC via the sensing of bacterial RNA, further emphasizing the importance of mitochondrial alterations in innate immunity (Garaude et al., 2016).

It was interesting to note that dimethyl fumarate, a cell-permeable fumarate ester, which has recently been approved as the front-line drug for the treatment of relapsing-remitting multiple sclerosis (Miljković et al., 2015), boosted both LPS-induced IL-1β expression and TNF-α production. These effects were somewhat surprising, as dimethyl fumarate has been suggested to exert its beneficial effects in disease largely by decreasing neuroinflammation. It has been shown to decrease ROS production in macrophages (Haas et al., 2015), most likely as a consequence of its effects on anti-oxidants, such as heme oxygenase-1, superoxide dismutase-2, and nuclear factor erythroid-2-related factor 2 (Nrf2), and to decrease IL-1β mRNA expression in microglial cells (Wilms et al., 2010). However, it is known that fumarate can stabilize HIF-1α, and this is likely the mechanism by which it is inducing IL-1β (Isaacs et al., 2005). Similarly, there may be an as-yet-unknown factor by which fumarate boosts TNF-α production, or this may be a result of epigenetic alterations of the TNF-α gene, which have been reported elsewhere (Sullivan et al., 2007; Xiao et al., 2012).

There are a number of possible sources for the ROS signal emanating from mitochondria in response to succinate oxidation and an elevated membrane potential, including from complex I and complex III (Chandel et al., 2000). We favor the hypothesis that the ROS signal is generated by reverse electron transport (RET) at complex I of the ETC. Complex I can produce large amounts of ROS by the precisely regulated process of RET when the CoQ pool is highly reduced and the mitochondrial membrane potential is high, together providing the thermodynamic driving force to push electrons in reverse to the ROS-producing site within complex I (Chance and Hollunger, 1961). Importantly, succinate has long been known to drive RET and recently has been shown to generate ROS production by RET during ischemia-reperfusion (I/R) injury (Chouchani et al., 2014). The data we present in this study indicate that the ROS signal is sensitive to uncoupling with CCCP, prevention of succinate oxidation by DMM, oxidation of the CoQ pool by expression of AOX (Perales-Clemente et al., 2008), and inhibition of complex I with rotenone, all of which are consistent with RET at complex I as the source of the pro-inflammatory ROS signal in LPS-activated macrophages. The decrease in LPS-induced ROS with the complex I inhibitor rotenone is particularly intriguing, as this inhibitor only lowers ROS by complex I if RET is occurring (Votyakova and Reynolds, 2001) and otherwise induces ROS production (Barrientos and Moraes, 1999). The role of RET in metabolic signaling has been implicated in a number of recent studies, such as I/R injury (Chouchani et al., 2014), mitochondrial ROS production during aging in *Drosophila* (Scialò et al., 2016), and hypoxia sensing in the carotid body (Fernández-Agüera et al., 2015). Furthermore, previous reports demonstrated that metformin, which inhibits complex I, decreases IL-1β in response to LPS (Kelly et al., 2015). Also of interest is the recent identification of TLR4 as a driver of ROS and subsequent systemic inflammation in mice deficient in the complex I subunit Ndufs4 (Jin et al., 2014), further emphasizing modulation of complex I by TLR4. While further work is required to assess the source of mitochondrial ROS during macrophage activation, we feel that RET at complex I is a strong candidate.

This central role for mitochondria in immune signaling and the innate immune response fits with the function of this organelle in many other aspects of cell death and signaling. Indeed, the endosymbiotic origins of mitochondria may reflect not only the requirement for eukaryotes to evolve to respire oxidatively but

(I–M)Wild-type and AOX-expressing BMDMs were untreated (Ctl) or pretreated for 3 hr with succinate (Suc; 5 mM; I and M) before being stimulated with LPS (100 ng/μL, I and K–M; or 1 μg/mL, J) for 48 hr.

(B, G, I, and M) Whole-cell lysates were analyzed by western blotting for pro-IL-1β, HIF-1α, β-actin and AOX.

(F) mRNA was extracted from total cell lysates and analyzed by qPCR for IL-1β expression.

(H) Supernatants were analyzed by ELISA for TNF-α production.

(J–L) Live cells were analyzed by FACS, and mean fluorescence intensity (MFI) was quantified as a measure of cellular reactive oxygen species production (J), or cells were costained with TMRM (20 nM) and MitoTracker Green (50 nM) for 30 min and then analyzed by FACS to quantify the membrane potential (K and L). The intensity of TMRM staining reflects the membrane potential. The cytometric dot plots in (L) are representative of five independent experiments.

(N) Wild-type (WT) and alternative oxidase (AOX)-expressing mice were injected i.p. with LPS (10 mg/kg), and the survival rate was monitored. AOX group, n = 11; WT group, n = 12.

The data in (A), (C)–(F), and (H) represent mean ± SEM, n = 3, or n = 5 for (J) and (K); *$p < 0.05$, **$p < 0.01$, ***$p < 0.001$. The blots in (B), (G), (I), and (M) are representative of three independent experiments. See also Figure S6.

also the idea that these organelles might have evolved to serve as signaling hubs, which can influence the phenotype of immune cells, and possibly other cell types, to aid in the response to infection.

Finally, the finding that succinate oxidation is an important regulator of inflammatory signaling opens up a number of new therapeutic opportunities. For example, DMM may be useful in the treatment of inflammatory diseases in which IL-1β has been linked to pathogenesis (Dinarello, 2011). Promisingly, inhibition of SDH with DMM has shown efficacy here in a mouse model of acute LPS-induced sepsis and previously in mouse models of *Escherichia coli* infection (Garaude et al., 2016) and I/R injury (Chouchani et al., 2014). Treatment with DMM or derivatives may therefore improve disease outcome by restoring the balance between IL-1β and IL-1RA or indeed by increasing IL-10 production, which can both decrease IL-1β and enhance IL-1RA levels (Cassatella et al., 1994) and suppress inflammation more generally (Couper et al., 2008). The shift in macrophages away from inflammatory gene expression toward anti-inflammatory gene expression within an inflammatory environment (such as in our LPS model) is especially noteworthy, since such an environment will prevail in inflammatory diseases, where inhibitors of SDH might prove especially useful.

STAR★METHODS

Detailed methods are provided in the online version of this paper and include the following:

- KEY RESOURCES TABLE
- CONTACT FOR REAGENT AND RESOURCE SHARING
- EXPERIMENTAL MODEL AND SUBJECT DETAILS
  - Mouse Strains
  - Bone Marrow-Derived Macrophage Generation
  - Endotoxin-Induced Model of Sepsis
- METHOD DETAILS
  - Real-Time PCR
  - Western Blotting
  - Enzyme-Linked Immunosorbent Assay
  - Flow Cytometric Analysis of Reactive Oxygen Species
  - NAD^+/NADH Measurement
  - ATP/ADP Measurement
  - Cytotoxicity Assay
  - Metabolite Measurements
  - Oxygen Consumption and Lactate Production Analysis
  - Mitochondrial Membrane Potential
  - In Vitro Deletion of SDHB
- QUANTIFICATION AND STATISTICAL ANALYSIS
  - Statistical Analysis
  - Transcriptomics Analysis
- DATA AND SOFTWARE AVAILABILITY
  - Software
  - Data Resources

SUPPLEMENTAL INFORMATION

Supplemental Information includes six figures and seven tables and can be found with this article online at http://dx.doi.org/10.1016/j.cell.2016.08.064.

AUTHOR CONTRIBUTIONS

E.L.M. and B.K. designed and performed experiments and analyzed the data. E.L.M. wrote the manuscript. A.L. performed and analyzed experiments measuring the membrane potential. A.S.H.C. and C.F. performed the LC-MS based metabolomics analysis. S.C.C. assisted with the in vivo LPS trial. D.R. assisted in experiments comparing the effects of Krebs cycle metabolites on LPS-induced cytokines. G.M. aided in confocal microscopy experiments. C.E.B. provided advice for the in vivo studies. J.H.M.D. and E.G. provided the SDHB-deficient bones. M.V. performed the RNA-sequencing analysis. I.L. coordinated RNA sequencing work. R.J.X. provided guidance and advice. T.B., H.T.J., and M.S. generated the AOX strain, conceived and performed the LPS-induced sepsis study in AOX mice, delivered the data, and provided AOX-expressing bones and associated reagents. M.P.M. provided advice and reagents and oversaw a portion of the work. L.A.O. conceived ideas and oversaw the research program.

ACKNOWLEDGMENTS

We thank Henry Däbritz (Cancer Metabolism Research Unit, Cancer Research UK, Beatson Institute, Bearsden, Glasgow) for bones from SDHB floxed mice. We thank Ariel Lefkovith and Bihua Li for their contribution to the library preparation for the RNA-sequencing analysis. We thank Praveen K. Dhandapani and Kira Holmström for assisting with the provision of the AOX mouse tissues. We thank Moritz Haneklaus for assistance with graphics.

This work was supported by funds and grants from the UK MRC MC_U105663142 (to M.P.M.), The Wellcome Trust (grant number 110159/Z/15/Z to M.P.M.), and Science Foundation Ireland (grant number [12/IA/1531]), the European Research Council, The Wellcome Trust (oneill-wellcome-trust-metabolic), and the Irish Research Council (to L.A.O.). Funding was provided by Academy of Finland (CoE grant 272376 to H.T.J.), the European Research Council (advanced grant 232738 to H.T.J.), the Tampere University Hospital Medical Research Fund, and the Sigrid Juselius Foundation (to H.T.J.). C.F. and A.S.H.C. were supported by an MRC Core Fund to the MRC Cancer Unit.

M.P.M. and C.F. have a patent application on the therapeutic application of SDH inhibitors.

Received: April 25, 2016
Revised: July 20, 2016
Accepted: August 25, 2016
Published: September 22, 2016

REFERENCES

Anders, S., Pyl, P.T., and Huber, W. (2015). HTSeq–a Python framework to work with high-throughput sequencing data. Bioinformatics *31*, 166–169.

Barrientos, A., and Moraes, C.T. (1999). Titrating the effects of mitochondrial complex I impairment in the cell physiology. J. Biol. Chem. *274*, 16188–16197.

Cassatella, M.A., Meda, L., Gasperini, S., Calzetti, F., and Bonora, S. (1994). Interleukin 10 (IL-10) upregulates IL-1 receptor antagonist production from lipopolysaccharide-stimulated human polymorphonuclear leukocytes by delaying mRNA degradation. J. Exp. Med. *179*, 1695–1699.

Chance, B., and Hollunger, G. (1961). The interaction of energy and electron transfer reactions in mitochondria. I. General properties and nature of the products of succinate-linked reduction of pyridine nucleotide. J. Biol. Chem. *236*, 1534–1543.

Chandel, N.S., McClintock, D.S., Feliciano, C.E., Wood, T.M., Melendez, J.A., Rodriguez, A.M., and Schumacker, P.T. (2000). Reactive oxygen species generated at mitochondrial complex III stabilize hypoxia-inducible factor-1alpha during hypoxia: a mechanism of O2 sensing. J. Biol. Chem. *275*, 25130–25138.

Chouchani, E.T., Pell, V.R., Gaude, E., Aksentijević, D., Sundier, S.Y., Robb, E.L., Logan, A., Nadtochiy, S.M., Ord, E.N., Smith, A.C., et al. (2014).

Ischaemic accumulation of succinate controls reperfusion injury through mitochondrial ROS. Nature *515*, 431–435.

Chouchani, E.T., Pell, V.R., James, A.M., Work, L.M., Saeb-Parsy, K., Frezza, C., Krieg, T., and Murphy, M.P. (2016). A unifying mechanism for mitochondrial superoxide production during ischemia-reperfusion injury. Cell Metab. *23*, 254–263.

Couper, K.N., Blount, D.G., and Riley, E.M. (2008). IL-10: the master regulator of immunity to infection. J. Immunol. *180*, 5771–5777.

Dervartanian, D.V., and Veeger, C. (1964). Studies on succinate dehydrogenase. I. Spectral properties of the purified enzyme and formation of enzyme-competitive inhibitor complexes. Biochim. Biophys. Acta *92*, 233–247.

Dinarello, C.A. (2011). Interleukin-1 in the pathogenesis and treatment of inflammatory diseases. Blood *117*, 3720–3732.

El-Khoury, R., Kemppainen, K.K., Dufour, E., Szibor, M., Jacobs, H.T., and Rustin, P. (2014). Engineering the alternative oxidase gene to better understand and counteract mitochondrial defects: state of the art and perspectives. Br. J. Pharmacol. *171*, 2243–2249.

Everts, B., Amiel, E., van der Windt, G.J., Freitas, T.C., Chott, R., Yarasheski, K.E., Pearce, E.L., and Pearce, E.J. (2012). Commitment to glycolysis sustains survival of NO-producing inflammatory dendritic cells. Blood *120*, 1422–1431.

Everts, B., Amiel, E., Huang, S.C., Smith, A.M., Chang, C.H., Lam, W.Y., Redmann, V., Freitas, T.C., Blagih, J., van der Windt, G.J., et al. (2014). TLR-driven early glycolytic reprogramming via the kinases TBK1-IKKε supports the anabolic demands of dendritic cell activation. Nat. Immunol. *15*, 323–332.

Fernández-Agüera, M.C., Gao, L., González-Rodríguez, P., Pintado, C.O., Arias-Mayenco, I., García-Flores, P., García-Pergañeda, A., Pascual, A., Ortega-Sáenz, P., and López-Barneo, J. (2015). Oxygen sensing by arterial chemoreceptors depends on mitochondrial complex I signaling. Cell Metab. *22*, 825–837.

Fernandez-Ayala, D.J., Sanz, A., Vartiainen, S., Kemppainen, K.K., Babusiak, M., Mustalahti, E., Costa, R., Tuomela, T., Zeviani, M., Chung, J., et al. (2009). Expression of the Ciona intestinalis alternative oxidase (AOX) in Drosophila complements defects in mitochondrial oxidative phosphorylation. Cell Metab. *9*, 449–460.

Garaude, J., Acín-Pérez, R., Martínez-Cano, S., Enamorado, M., Ugolini, M., Nistal-Villán, E., Hervás-Stubbs, S., Pelegrín, P., Sander, L.E., Enríquez, J.A., and Sancho, D. (2016). Mitochondrial respiratory-chain adaptations in macrophages contribute to antibacterial host defense. Nat. Immunol. *17*, 1037–1045.

Guarda, G., Braun, M., Staehli, F., Tardivel, A., Mattmann, C., Förster, I., Farlik, M., Decker, T., Du Pasquier, R.A., Romero, P., and Tschopp, J. (2011). Type I interferon inhibits interleukin-1 production and inflammasome activation. Immunity *34*, 213–223.

Guzy, R.D., Sharma, B., Bell, E., Chandel, N.S., and Schumacker, P.T. (2008). Loss of the SdhB, but Not the SdhA, subunit of complex II triggers reactive oxygen species-dependent hypoxia-inducible factor activation and tumorigenesis. Mol. Cell. Biol. *28*, 718–731.

Haas, B., Chrusciel, S., Fayad-Kobeissi, S., Dubois-Randé, J.L., Azuaje, F., Boczkowski, J., Motterlini, R., and Foresti, R. (2015). Permanent culture of macrophages at physiological oxygen attenuates the antioxidant and immunomodulatory properties of dimethyl fumarate. J Cell Physiol. *230*, 1128–1138.

Hamanaka, R.B., Weinberg, S.E., Reczek, C.R., and Chandel, N.S. (2016). The mitochondrial respiratory chain is required for organismal adaptation to hypoxia. Cell Rep. *15*, 451–459.

Isaacs, J.S., Jung, Y.J., Mole, D.R., Lee, S., Torres-Cabala, C., Chung, Y.L., Merino, M., Trepel, J., Zbar, B., Toro, J., et al. (2005). HIF overexpression correlates with biallelic loss of fumarate hydratase in renal cancer: novel role of fumarate in regulation of HIF stability. Cancer Cell *8*, 143–153.

Jha, A.K., Huang, S.C., Sergushichev, A., Lampropoulou, V., Ivanova, Y., Loginicheva, E., Chmielewski, K., Stewart, K.M., Ashall, J., Everts, B., et al. (2015). Network integration of parallel metabolic and transcriptional data reveals metabolic modules that regulate macrophage polarization. Immunity *42*, 419–430.

Jin, Z., Wei, W., Yang, M., Du, Y., and Wan, Y. (2014). Mitochondrial complex I activity suppresses inflammation and enhances bone resorption by shifting macrophage-osteoclast polarization. Cell Metab. *20*, 483–498.

Kato, M. (1972). Site of action of lipid A on mitochondria. J. Bacteriol. *112*, 268–275.

Kelly, B., Tannahill, G.M., Murphy, M.P., and O'Neill, L.A. (2015). Metformin inhibits the production of reactive oxygen species from NADH:ubiquinone oxidoreductase to limit induction of IL-1β and boosts IL-10 in LPS-activated macrophages. J. Biol. Chem. *290*, 20348–20359.

Kelso, G.F., Porteous, C.M., Coulter, C.V., Hughes, G., Porteous, W.K., Ledgerwood, E.C., Smith, R.A., and Murphy, M.P. (2001). Selective targeting of a redox-active ubiquinone to mitochondria within cells: antioxidant and antiapoptotic properties. J. Biol. Chem. *276*, 4588–4596.

Langmead, B., Trapnell, C., Pop, M., and Salzberg, S.L. (2009). Ultrafast and memory-efficient alignment of short DNA sequences to the human genome. Genome Biol. *10*, R25.

McGivney, A., and Bradley, S.G. (1979). Action of bacterial endotoxin and lipid A on mitochondrial enzyme activities of cells in culture and subcellular fractions. Infect. Immun. *25*, 664–671.

Miljković, D., Blaževski, J., Petković, F., Djedović, N., Momčilović, M., Stanisavljević, S., Jevtić, B., Mostarica Stojković, M., and Spasojević, I. (2015). A comparative analysis of multiple sclerosis-relevant anti-inflammatory properties of ethyl pyruvate and dimethyl fumarate. J Immunol. *194*, 2493–2503.

Mills, E.L., and O'Neill, L.A. (2016). Reprogramming mitochondrial metabolism in macrophages as an anti-inflammatory signal. Eur. J. Immunol. *46*, 13–21.

O'Neill, L.A., and Pearce, E.J. (2016). Immunometabolism governs dendritic cell and macrophage function. J. Exp. Med. *213*, 15–23.

Pello, O.M., De Pizzol, M., Mirolo, M., Soucek, L., Zammataro, L., Amabile, A., Doni, A., Nebuloni, M., Swigart, L.B., Evan, G.I., et al. (2012). Role of c-MYC in alternative activation of human macrophages and tumor-associated macrophage biology. Blood *119*, 411–421.

Perales-Clemente, E., Bayona-Bafaluy, M.P., Pérez-Martos, A., Barrientos, A., Fernández-Silva, P., and Enriquez, J.A. (2008). Restoration of electron transport without proton pumping in mammalian mitochondria. Proc. Natl. Acad. Sci. USA *105*, 18735–18739.

Scialò, F., Sriram, A., Fernández-Ayala, D., Gubina, N., Lõhmus, M., Nelson, G., Logan, A., Cooper, H.M., Navas, P., Enríquez, J.A., et al. (2016). Mitochondrial ROS Produced via Reverse Electron Transport Extend Animal Lifespan. Cell Metab. *23*, 725–734.

Sena, L.A., Li, S., Jairaman, A., Prakriya, M., Ezponda, T., Hildeman, D.A., Wang, C.R., Schumacker, P.T., Licht, J.D., Perlman, H., et al. (2013). Mitochondria are required for antigen-specific T cell activation through reactive oxygen species signaling. Immunity *38*, 225–236.

Sullivan, K.E., Reddy, A.B., Dietzmann, K., Suriano, A.R., Kocieda, V.P., Stewart, M., and Bhatia, M. (2007). Epigenetic regulation of tumor necrosis factor alpha. Mol. Cell. Biol. *27*, 5147–5160.

Tannahill, G.M., Curtis, A.M., Adamik, J., Palsson-McDermott, E.M., McGettrick, A.F., Goel, G., Frezza, C., Bernard, N.J., Kelly, B., Foley, N.H., et al. (2013). Succinate is an inflammatory signal that induces IL-1β through HIF-1α. Nature *496*, 238–242.

Trapnell, C., Pachter, L., and Salzberg, S.L. (2009). TopHat: discovering splice junctions with RNA-Seq. Bioinformatics *25*, 1105–1111.

Votyakova, T.V., and Reynolds, I.J. (2001). DeltaPsi(m)-Dependent and -independent production of reactive oxygen species by rat brain mitochondria. J. Neurochem. *79*, 266–277.

West, A.P., Brodsky, I.E., Rahner, C., Woo, D.K., Erdjument-Bromage, H., Tempst, P., Walsh, M.C., Choi, Y., Shadel, G.S., and Ghosh, S. (2011). TLR

signalling augments macrophage bactericidal activity through mitochondrial ROS. Nature *472*, 476–480.

Wilms, H., Sievers, J., Rickert, U., Rostami-Yazdi, M., Mrowietz, U., and Lucius, R. (2010). Dimethylfumarate inhibits microglial and astrocytic inflammation by suppressing the synthesis of nitric oxide, IL-1beta, TNF-alpha and IL-6 in an in-vitro model of brain inflammation. J Neuroinflammation *7*, 30.

Xiao, M., Yang, H., Xu, W., Ma, S., Lin, H., Zhu, H., Liu, L., Liu, Y., Yang, C., Xu, Y., et al. (2012). Inhibition of α-KG-dependent histone and DNA demethylases by fumarate and succinate that are accumulated in mutations of FH and SDH tumor suppressors. Genes Dev. *26*, 1326–1338.

Yang, M., and Pollard, P.J. (2013). Succinate: a new epigenetic hacker. Cancer Cell *23*, 709–711.

STAR★METHODS

KEY RESOURCES TABLE

REAGENT or RESOURCE	SOURCE	IDENTIFIER
Antibodies		
Goat anti-mouse IL-1β	R&D Systems	Cat# AF-401-NA; RRID: AB_416684
Rabbit anti-HIF-1α	Novus	Cat# NB100-449; RRID: AB_10001045
Rabbit anti-phospho-NFκB p65	Cell Signaling Technology	Cat# 3033S
Rabbit anti-NFκB p65	Cell Signaling Technology	Cat# 8242S; RRID: 10860244
Rabbit anti-IκBα	Cell Signaling Technology	Cat# 4812S; RRID: AB_10694416
Rabbit anti-AOX	Laboratory of Howy Jacobs, Fernandez-Ayala et al., 2009	N/A
Purified NA/LE rat anti-mouse CD210 Clone 1B1.3a (RUO)	BD Biosciences	Cat# 550012; RRID: AB_393532
Purified NA/LE rat IgG1 κ isotype control Clone R3-34 (RUO)	BD Biosciences	Cat# 554682; RRID AB_395507
Chemicals, Peptides, and Recombinant Proteins		
Lipopolysaccharide from *Escherichia coli*, serotype EH100	Alexis	Cat# ALX-158-010
Lipopolysaccharide from *Escherichia coli*, serotype O55:B5	Sigma-Aldrich	Cat# L2880
Alpha-ketoglutarate	Sigma-Aldrich	Cat# 349631, CAS: 13192-04-6
Carbonyl cyanide *m*-chlorophenyl hydrazine	Sigma-Aldrich	Cat# C2759; CAS: 555-60-2
2-deoxyglucose	Sigma-Aldrich	Cat# D3179; CAS: 154-17-6
Diethyl succinate	Sigma-Aldrich	Cat# 112402; CAS: 123-25-1
Diethyl butyl malonate	Sigma-Aldrich	Cat# 112038; CAS: 133-08-4
Dimethyl malonate	Sigma-Aldrich	Cat# 136441; CAS: 108-59-8
Dimethyloxalylglycine	Cayman Chemicals	Cat# 71210; CAS: 89464-63-1
Dimethyl fumarate	Santa Cruz Biotechnology	Cat# sc-239774; CAS: 624-49-7
Methyl pyruvate	Sigma-Aldrich	Cat# 371173; CAS: 600-22-6
MitoTEMPO	Sigma-Aldrich	Cat# SML0737; CAS: 1334850-99-5
Triethyl citrate	Sigma-Aldrich	Cat# 14849; CAS: 77-93-0
Oligomycin A	Sigma-Aldrich	Cat# 75351; CAS: 579-13-5
Rotenone	Sigma-Aldrich	Cat# R8875; CAS: 83-79-4
4-hydroxytamoxifen	Sigma-Aldrich	Cat# H7904; CAS: 68047-06-3
Antimycin A	Sigma-Aldrich	Cat# A8674; CAS: 1397-94-0
MitoQ	Laboratory of Rob Smith, Kelso et al., 2001	N/A
MitoSOX Red mitochondrial superoxide indicator	Molecular Probes	Cat# M36008
CellROX Deep Red	Molecular Probes	Cat# C10422
MitoTracker Green	Molecular Probes	Cat# M7514; CAS: 201860-17-5
Tetramethylrhodamine methyl ester (TMRM)	Molecular Probes	Cat# T668; CAS: 115532-50-8
Critical Commercial Assays		
ATP/ADP ratio assay kit	Sigma-Aldrich	Cat# MAK135
NAD^+/NADH quantification colorimetric kit	BioVision	Cat# K337
CytoTox96 non-radioactive cytotoxicity assay kit	Promega	Cat# G1780
Live/Dead Fixable Aqua dead cell stain kit	Molecular Probes	Cat# L34957
Mouse IL-10 ELISA Duoset	R&D Systems	Cat# DY417
Mouse TNF-α ELISA Duoset	R&D Systems	Cat# DY410E

(*Continued on next page*)

Continued		
REAGENT or RESOURCE	SOURCE	IDENTIFIER
Mouse IL-1β Quantikine ELISA kit	R&D Systems	Cat# MLB00C
Mouse IL-10 Quantikine ELISA kit	R&D Systems	Cat# M1000B
Mouse TNF-α Quantikine ELISA kit	R&D Systems	Cat# MTA00B
Deposited Data		
Raw and analyzed RNASeq data	This paper	GEO: GSE78849
Experimental Models: Organisms/Strains		
Mouse: AOX-overexpressing	Laboratory of Howy Jacobs. The AOX strain will be described in detail elsewhere.	N/A
Mouse: SDHB-deficient: ROSA26-CreER^{T2}/ SDHB$^{floxed/floxed}$	Laboratory of Eyal Gottlieb	N/A
Mouse: SDHB-proficient: ROSA26-CreER^{T2}/ SDHB$^{wildtype/wildtype}$	Laboratory of Eyal Gottlieb	N/A
Sequence-Based Reagents		
HIF-1α TaqMan assay	Applied Biosystems	Cat# 4331182; Assay ID: Mm00468869_m1
EGLN3 TaqMan assay	Applied Biosystems	Cat# 4331182; Assay ID: Mm00472200_m1
Rps18 FAM TaqMan assay	Applied Biosystems	Cat# 4331182; Assay ID: Mm_02601777_g1
Primers for mouse IL-1β	See Table S7	N/A
Primers for mouse IL-10	See Table S7	N/A
Primers for mouse TNF- α	See Table S7	N/A
Primers for mouse Rps18	See Table S7	N/A
Primers for mouse IL-1ra	See Table S7	N/A
Primers for mouse PHD3	See Table S7	N/A
Primers for mouse cMyc	See Table S7	N/A
Primers for mouse CD71	See Table S7	N/A
Software and Algorithms		
GraphPad Prism	GraphPad Software	http://www.graphpad.com/scientific-software/prism/
FlowJo	FlowJo	http://www.flowjo.com/
Bowtie	Langmead et al., 2009	http://bowtie-bio.sourceforge.net/index.shtml
TopHat	Trapnell et al., 2009	http://ccb.jhu.edu/software/tophat/index.shtml
HTSeq	Anders et al., 2015	https://pypi.python.org/pypi/HTSeq

CONTACT FOR REAGENT AND RESOURCE SHARING

Further queries and reagent requests may be directed and will be fulfilled by the lead contact, Luke A. O'Neill (laoneill@tcd.ie).

EXPERIMENTAL MODEL AND SUBJECT DETAILS

Mouse Strains

Wild-type C57Bl/6 mice were from Harlan UK and Harlan Netherlands. Animals (female; 8-12 weeks) were maintained under specific pathogen-free conditions in line with Irish and European Union regulations. Experiments were approved by local ethical review (Health Products Regulatory Authority) and were carried out under the authority of Ireland's project license. C57Bl/6 mice carrying a single copy of *Ciona intestinalis* AOX gene in the Rosa26 locus were generated by T. Braun, H. T. Jacobs and M. Szibor (full details to be published elsewhere). Animals (females; 22-37 weeks) were maintained under specific pathogen-free conditions. LPS experiments in AOX-expressing mice were carried out by Luria Scientific Industries under the IACUC Assurance number A7433J45. Legs from AOX-expressing mice were supplied by M. Szibor, H. T. Jacobs (both University of Helsinki, Finland) and M. P. Murphy (University of Cambridge, UK). Legs from SDHB-deficient mice (males and females; 8-22 weeks; maintained under specific pathogen-free conditions) were a gift from E. Gottlieb (University of Glasgow, UK).

Bone Marrow-Derived Macrophage Generation

Mice were euthanized in a CO_2 chamber and death was confirmed by cervical dislocation. Bone marrow cells were extracted from the leg bones and differentiated in DMEM (containing 10% fetal calf serum, 1% penicillin streptomycin and 20% L929 supernatant) for 6 days, at which time they were counted and replated for experiments. Unless stated, $0.5x10^6$ BMDMs per milliliter were used in in vitro experiments.

Endotoxin-Induced Model of Sepsis

Female C57/Bl6 mice (aged 7–9 weeks, weighing 13–20 g) were randomly assigned to experimental groups (5 mice per group). Mice were treated i.p. ± dimethyl malonate (160 mg/kg) or PBS for 3 hr prior to stimulation with LPS (15 mg/kg) i.p. for 2 hr. Mice were euthanized in a CO_2 chamber and peritoneal cells, spleens, and whole blood samples were harvested. AOX-expressing mice were treated i.p. with LPS (10 mg/kg) on day 0 and then followed up for seven days.

METHOD DETAILS

Real-Time PCR

Total RNA was isolated using the RNeasy Plus Mini kit (QIAGEN) and quantified using a Nanodrop 2000 UV-visible spectrophotometer. cDNA was prepared using 20–100 ng/μl total RNA by a RT-PCR using a high capacity cDNA reverse transcription kit (Applied Biosystems), according to the manufacturer's instructions. Real-time qPCR was performed on cDNA using SYBR Green probes specific for IL-1β, IL-10, TNF-α, IL-1RA and Rps18, or TaqMan probes specific for HIF-1α, PHD3 and Rps18. Details on the primers used can be found in Table S7. qPCR was performed on a 7900 HT Fast Real-Time PCR System (Applied Biosystems) using Kapa fast master mix high ROX (Kapa Biosystems, for SYBR probes) or 2X PCR fast master mix (Applied Biosystems, for TaqMan probes). Primer Sequences for SYBR green real-time PCR are shown in Table S7. The SYBR primer pair sequences were as follows: *Il1b*, FW 5′-TGGCAACTGTTCCTG-3′, RV 5′-GGAAGCAGCCCTTCATCTTT-3′; *Il10*, FW 5′-AGGCGCTGTCATCGATTT-3′, RV 5′-CACC TTGGTCTTGGAGCTTAT-3′; *Tnfa*, FW 5′-GCCTCTTCTCATTCCTGCTT-3′, RV 5′-TGGGAACTTCTCATCCCTTTG-3′; *Rps18*, FW 5′-GGATGTGAAGGATGGGAAGT-3′, RV 5′-CCCTCTATGGGCTCGAATTT-3′; *Il-1ra*, FW 5′-TTGTGCCAAGTCTGGAGATG-3′, RV 5′-CTCAGAGCGGATGAAGGTAAAG-3′; *Phd3*, FW 5′-TGCTGAAGAAAGGGCAGAAG-3′; RV 5′-GCACACCACAGTCAGTCTTTA −3′; *cMyc*, FW 5′-CCACCAGCAGCGACTCTG-3′, RV 5′-GAGATGAGCCCGACTCCG-3′; *CD71*, FW 5′-AAGTGACGTAGATCCAGAGGG-3′, RV 5′-GACAATGGTTCCCCACCAAA-3′. Fold changes in expression were calculated by the Delta Delta Ct method using mouse Rps18 as an endogenous control for mRNA expression. All fold changes are expressed normalized to the untreated control.

Western Blotting

Protein samples from cultured cells were prepared by direct lysis of cells in 5X Laemmli sample buffer, followed by heating at 95°C for 5 min. For spleen samples, 30 mg of spleen was homogenized in RIPA buffer using the QIAGEN TissueLyserII system. The resulting homogenate was centrifuged at 14000 rpm for 10 min at 4°C, and supernatants were used for SDS-PAGE. Protein samples were resolved on 8% or 12% SDS-PAGE gels and were then transferred onto polyvinylidene difluoride (PVDF) membrane using either a wet or semi-dry transfer system. Membranes were blocked in 5% (w/v) dried milk in Tris-buffered saline-Tween (TBST) for at least one hour at room temperature. Membranes were incubated with primary antibody, followed by the appropriate horseradish peroxidase-conjugated secondary antibody. They were developed using LumiGLO enhanced chemiluminescent (ECL) substrate (Cell Signaling). Bands were visualized using the GelDoc system (Bio-Rad).

Enzyme-Linked Immunosorbent Assay

Cytokine concentrations in cell supernatants were measured using ELISA Duoset kits for mouse IL-10 and TNF-α, according to the manufacturer's instructions. Cytokine concentrations in serum samples isolated from whole blood were measured using Quantikine ELISA kits for mouse IL-1β, IL-10 and TNF-α. Duoset and Quantikine kits were from R&D Systems. Optical density values were measured at a wavelength of 450 nm, using a FLUOstar Optima plate reader (BMG Labtech). Concentrations were calculated using a 4-parameter fit curve.

Flow Cytometric Analysis of Reactive Oxygen Species

BMDMs were seeded at $0.5x10^6$ cells/ml. One well was seeded for each of the following controls: unstained cells, single-stained cells and dead cells. For cellular reactive oxygen species (ROS) measurements cells were treated and stimulated as normal. 2 hr prior to staining, 100% EtOH was added to the dead cell control well. 30 min prior to the end of the stimulation, CellROX (5 μM) was added directly into the cell culture medium. Supernatants of cells that were to be stained with Aqua Live/Dead were removed, and an Aqua Live/Dead dilution (1 ml; 1 in 1000 in PBS) was added to each well. Cells were incubated in tinfoil at 37°C for 30 min. For mitoROS measurements MitoSOX (5 μM) and Aqua Live/Dead were each added for 30 min prior to stimulation. The media was then removed and replaced with stimulus-containing media. The supernatant was removed and cells were scraped in PBS (1 ml), before being transferred to polypropylene FACS tubes. Cells were centrifuged at 2000 rpm for 3 min. Cells were washed in PBS and centrifuged two further times, and were finally resuspended in PBS (500 μl). BMDMs were analyzed using a Dako CyAn flow cytometer, and data were analyzed using FlowJo software.

NAD^+/NADH Measurement

BMDMs were plated at $0.5x10^6$ cells/ml in 10 cm non-cell culture-treated dishes (10 ml/dish) and treated as required. NAD^+/NADH was assayed using an NAD^+/NADH quantification colorimetric kit (BioVision) according to the manufacturer's instructions.

ATP/ADP Measurement

BMDMs were plated at $0.5x10^6$ cells/ml in white 96-well plates (100 μl/well) and treated as required. ATP/ADP was assayed using an ATP/ADP quantification bioluminescent kit (Sigma) according to the manufacturer's instructions.

Cytotoxicity Assay

To determine cytotoxicity, cells were plated at $0.5x10^6$ cells/ml in white 24-well plates (500 μl/well) and treated as required. Cytotoxicity, as determined by LDH release, was assayed using CytoTox96 Non-radioactive Cytotoxicity Assay kit (Promega) according to the manufacturer's instructions.

Metabolite Measurements

Intracellular Metabolites

Cells were washed three times with ice-cold PBS, with all of the PBS being removed after the last wash. EB was added (1 ml per $1x10^6$ cells). Samples were agitated for 15 min at 4°C. The resultant suspension was transferred to ice-cold microcentrifuge tubes and centrifuged at maximum speed for 10 min at 4°C. The supernatant was transferred into autosampler vials and stored at −80°C prior to analysis by LC-MS.

Samples were randomized in order to avoid bias due to machine drift. LC-MS analysis of sample extracts was performed on a QExactive Orbitrap mass spectrometer coupled to a Dionex UltiMate 3000 Rapid Separation LC system (Thermo). The liquid chromatography system was fitted with a SeQuant Zic-HILIC (150 mm × 4.6 mm, 5 μm) with guard column (20 mm × 2.1 mm, 5 μm) from Merck (Darmstadt, Germany). The mobile phase was composed of 0.1% formic acid in water (solvent A), and 0.1% formic acid in acetonitrile (solvent B), and the flow rate set at 300 $\mu l \times min^{-1}$. The mass spectrometer was operated in full MS and polarity switching mode. Samples were randomized in order to avoid machine drift, and blinded to the operator. The acquired spectra were analyzed using XCalibur Qual Browser and XCalibur Quan Browser software (Thermo Scientific) by referencing to an internal library of compounds.

Oxygen Consumption and Lactate Production Analysis

Cells were plated at $0.2x10^6$ cells/well of a 24-well Seahorse plate with one well per row of the culture plate containing only supplemented media without cells, as a negative control. Cells were treated and stimulated as normal. A utility plate containing calibrant solution (1 ml/well) together with the plates containing the injector ports and probes was placed in a CO_2-free incubator at 37°C overnight. The following day media was removed from cells and replaced with glucose-supplemented XF assay buffer (500 μl/well) and the cell culture plate was placed in a CO_2-free incubator for at least 0.5 hr. Inhibitors (Oligomycin, carbonyl cyanide-*4*-(trifluoromethoxy)phenylhydrazone (FCCP), 2DG, Rotenone; 70 μl) were added to the appropriate port of the injector plate. This plate together with the utility plate was run on the Seahorse for calibration. Once complete, the utility plate was replaced with the cell culture plate and run on the Seahorse XF-24.

Mitochondrial Membrane Potential

Confocal Microscopy

Cells were plated at $0.3x10^6$ cells/ml in DMEM containing 10% FCS and 1% P/S in CELLview cell culture dishes containing four compartments per dish (500 μl/compartment). TMRM cell-permeable fluorescent dye was either added before or after stimulation depending on the length and nature of treatment. In the case of LPS-treated cells following stimulation media was removed and replaced with TMRM-containing media (20 nM) and incubated at 37° in the dark for 30 min. Oligomycin or CCCP was added after the addition of TMRM for 1 hr or 2 min respectively. Cells were imaged on a Leica SP8 confocal microscope with an excitation laser of 550 nm and detection set for 560-650 nM using a 40x oil-objective lens. A number of images were taken for each treatment.

Flow Cytometry

Cells were plated at $0.5x10^6$ cells/ml in 12-well plates. The following control cell samples were accounted for: unstained, single-stained TMRM, MitoTracker Green (MTG) and Aqua Live/Dead stain and 100% dead cells (treated with 100% ethanol for 1 h). Cells were prepared and treated as normal. TMRM stock was made up in DMSO (10 mM). MTG and Aqua Live/Dead stain were prepared by the addition of DMSO (75 μl or 50 μl/vial respectively). Supernatants were removed from all cells that were to be stained with Aqua Live/Dead (i.e., all samples except single-stained and unstained controls) and this was replaced with PBS (1 ml) containing Aqua Live/Dead stain (1 μl) and incubated at 37°C in the dark for 30 min. A mix of PBS containing MTG (50 nM) and TMRM (20 nM) was made up. Supernatant was removed from cells to be stained with MTG and TMRM (i.e., all samples except single-stained and unstained controls) and this was replaced with PBS containing MTG and TMRM (1 ml) and incubated at 37°C in the dark for 30 min. Supernatants were removed and cells were washed with PBS (1 ml). PBS (500 μL) was added per well and cells were removed from the plate surface using a cell scraper and transferred to polypropylene FACS tubes. Cells were then analyzed using a LSRFortessa flow cytometer, and data were analyzed using FlowJo software.

In Vitro Deletion of SDHB

BMDMs from mice carrying a SDHB fl/fl allele were utilized. Ablation of SDHB was achieved by adding 4-hydroxytamoxifen (600 nM) on day 4 of macrophage differentiation and again for a further 24 hr when cells were replated on day 6. Ethanol was used as a vehicle control for the 4-hydroxytamoxifen treatment.

QUANTIFICATION AND STATISTICAL ANALYSIS

Statistical Analysis

Comparisons between two groups were calculated using one- or two-tailed Student's t tests, using GraphPad Prism software. Data are reported as mean ± SEM. Statistical values, including number of replicates (n), can be found in the figure legends. *$p < 0.05$, **$p < 0.01$, ***$p < 0.001$. For in vitro experiments, n = number of separate experiments. For in vivo work, n = number of individual animals.

Transcriptomics Analysis

Total RNA was isolated using the RNeasy Plus Mini kit (QIAGEN) and quantified using a Nanodrop 2000 UV-visible spectrophotometer. cDNA libraries were generated using the Smart-seq2 protocol modified for 50 ng of total RNA input and sequenced on a MiSeq (Illumina, San Diego, CA) per manufacturer's instructions. Sequences obtained from the RNASeq pipeline were aligned against the *Mus musculus* genome using TopHat (Trapnell et al., 2009) + Bowtie (Langmead et al., 2009). HTSeq-count (Anders et al., 2015) was used to count the transcripts associated with each gene, and a counts matrix containing the number of counts for each gene across different samples and stimulations was obtained. The counts were normalized using the TMM method (http://dx.doi.org/10.1186/gb-2010-11-3-r25). To analyze differential expression across different stimulations, the counts matrix was fitted with a generalized linear model, using the edgeR package. A nested interaction model involving LPS stimulation and stimulation with DMM or succinate as the two factors was used to analyze the gene expression. Three comparisons were made using this model to explore in detail the effects of DMM and succinate on LPS-activated macrophages -

1. Differential gene expression under stimulation with LPS alone in the base case was compared to LPS stimulation when the samples were pretreated with DMM or succinate, and the strength and direction of regulation of expression by these two compounds was compared to the base case (Figure 3A). A list of genes which showed statistically significant regulation in opposite directions in both the base case and with pretreatment (e.g., genes found to have higher expression when stimulated with succinate + LPS compared with LPS alone, and lower expression with DMM + LPS compared with LPS alone) was obtained - and analyzed for biological pathway enrichment in the GO and KEGG databases (Figure 3B).
2. A direct comparison was made between LPS-activated macrophages pretreated with succinate and LPS-activated macrophages pretreated with DMM to find very high confidence pathways that were oppositely regulated under both comparisons (Figure 3C).
3. Further, samples which were treated with LPS at different time points (4 hr or 48 h) were analyzed separately to identify genes which were being expressed differently at different stages of the LPS stimulation (Figures S3K–S3M).

For all the comparisons, an FDR-adjusted p value of 0.05 was considered to be the threshold for statistical significance, where the Benjamini-Hochberg test was used for multiple testing correction.

DATA AND SOFTWARE AVAILABILITY

Software

GraphPad Prism was used for statistical analysis and graphing. Tophat and Bowtie were used to align sequences from the RNASeq pipeline against the *Mus musculus* genome. HTSeq-count was used to count the transcripts associated with each gene in the transcriptomics analysis. Details regarding acquisition of all software can be found in the Key Resources table.

Data Resources

The raw and processed RNASeq data have been deposited to PubMed GEO under GSE78849.

Cell

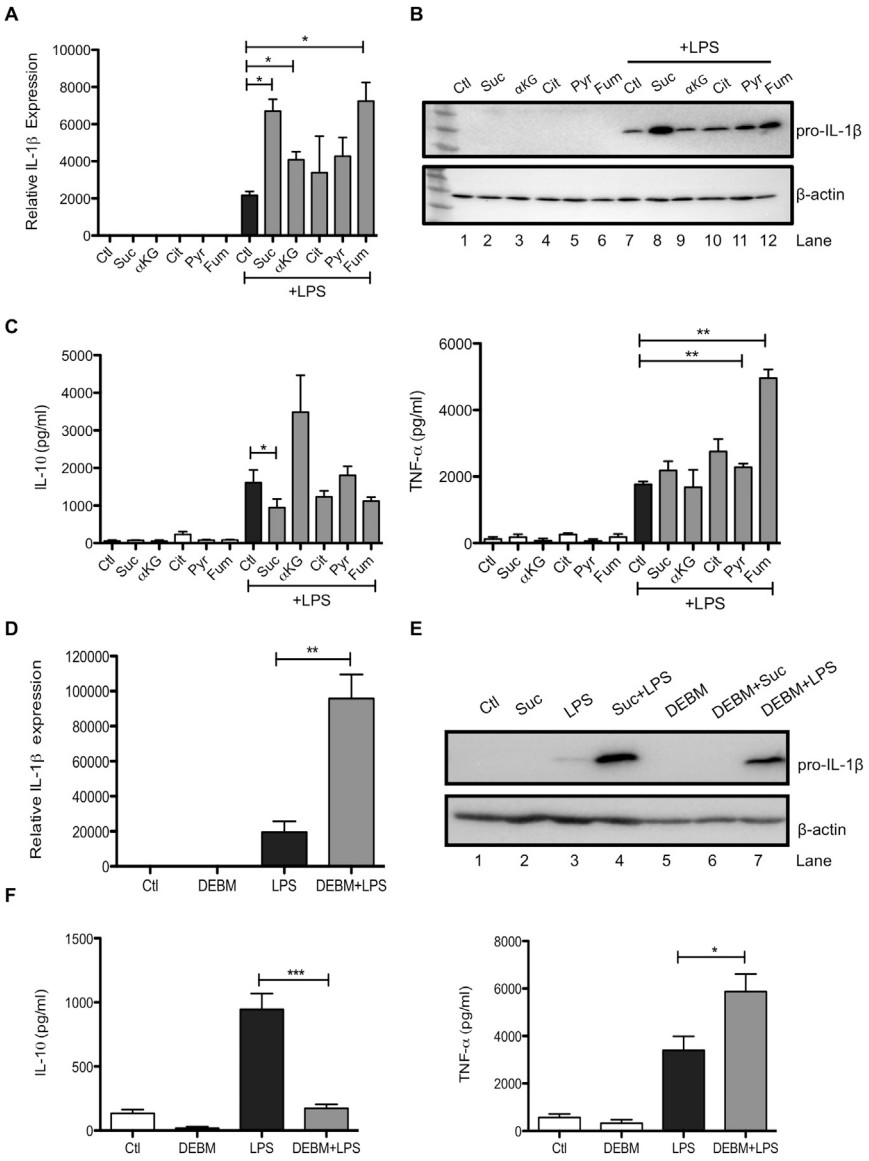

Figure S1. The Effect of Other Krebs Cycle Metabolites on LPS-Induced Cytokine Production, Related to Figure 1

(A–F) BMDMs were pretreated with a range of TCA cycle metabolites (succinate, Suc, 5 mM; α-ketoglutarate, αKG, 1 mM; citrate, Cit, 10 mM; pyruvate, Pyr, 5 mM; fumarate, Fum, 25 μM) or diethyl butylmalonate (DEBM; 1 mM) for 3 hr prior to stimulation with LPS (100 ng/ml) for 48 hr. Whole cell lysates were analyzed by western blotting for pro-IL-1β and β-actin (B, E). mRNA was extracted from total cell lysates and analyzed by qPCR for IL-1β (A, D) expression. Supernatants were analyzed by ELISA for IL-10 (C, F) and TNF-α production (C,F). The data in (A, C – D, F) represent mean ± SEM, n = 3, *p = 0.05, **p < 0.01, ***p < 0.001. The blots in (B, E) are representative of 3 independent experiments.

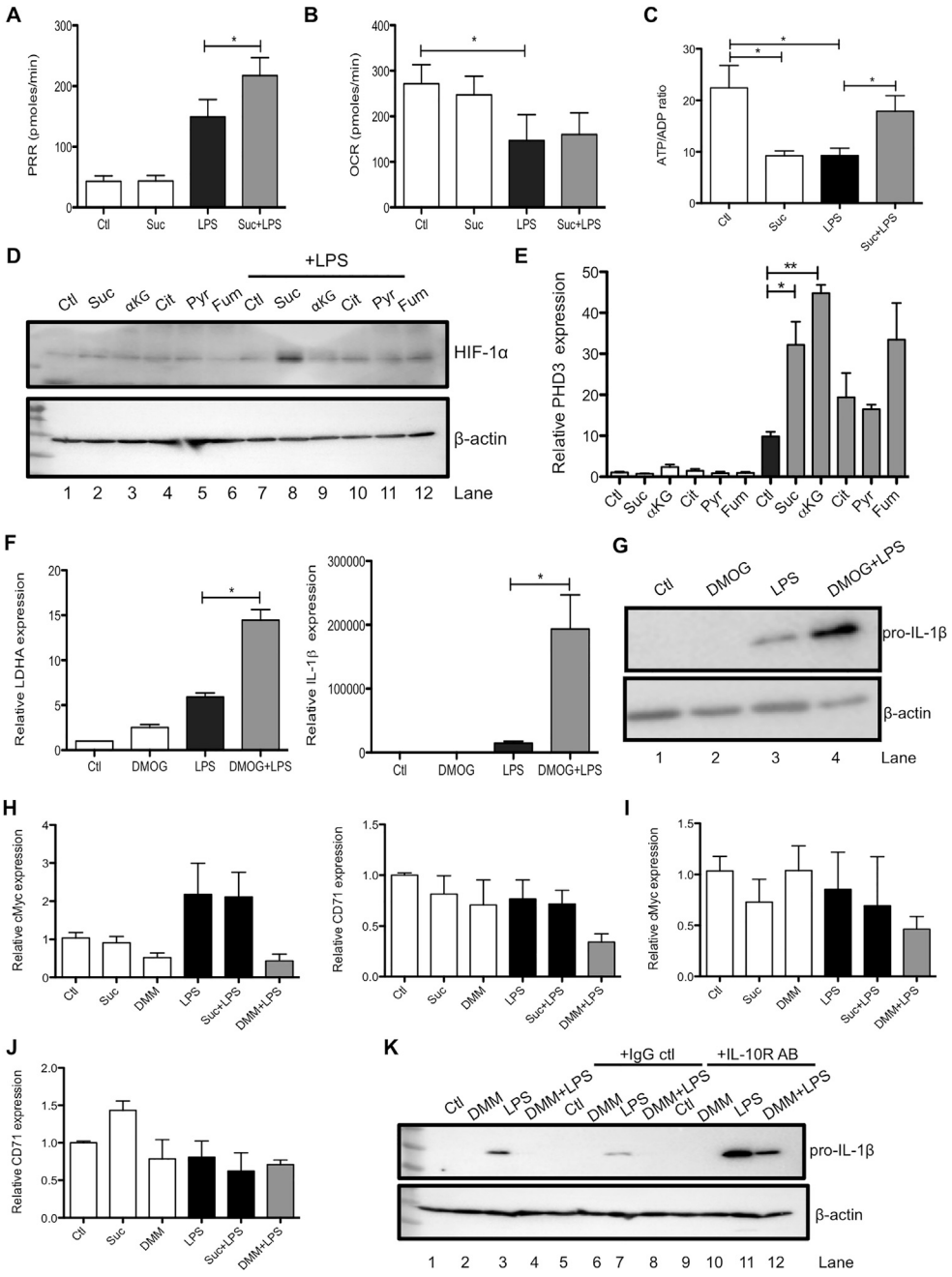

Figure S2. The Effects of Succinate May Be HIF-1α Dependent, but They Are Independent of cMyc and IL-10, Related to Figures 1 and 2

(A–K) BMDMs were pretreated with succinate (Suc; 5 mM) then stimulated with LPS (100 ng/ml) for 48 hr (A-C) and oxygen consumption rate (OCR) and proton production rate (PPR) were analyzed as read-outs for oxidative phosphorylation and glycolysis, respectively, using the Seahorse XF-24. The ATP/ADP ratio in cell lysates was determined using an ATP/ADP assay kit (C). BMDMs were pretreated with a range of TCA cycle metabolites (succinate, Suc, 5 mM; α-ketoglutarate, αKG, 1 mM; citrate, Cit, 10 mM; pyruvate, Pyr, 5 mM; fumarate, Fum, 25 μM) or with dimethyloxalylglcine (DMOG; 200 μM) for 3 hr prior to stimulation with LPS (100 ng/ml) for 48 hr (D – G, I, K) or 4 hr (H). BMDMs were untreated (Ctl) or pretreated with an IL-10 receptor blocking antibody (IL-10R AB; 10 μg/ml) or the appropriate isotype control (IgG ctl; 10 μg/ml) for 1 hr prior to the addition of dimethyl malonate (DMM; 10 mM; J) for 3 hr before stimulation with LPS (100 ng/ml) for 48 hr. Whole cell lysates were analyzed by western blotting for HIF-1α, pro-IL-1β and β-actin (D, G, K). mRNA was extracted from total cell lysates and analyzed by qPCR for PHD3 (E), LDHA (F), IL-1β (F), cMyc (H, I) and CD71 (H, J) expression. The data in (A - C, E, F, H, I, J) represent mean ± SEM, n = 3, *p = 0.05, **p < 0.01. The blots in (D, G, K) are representative of 3 independent experiments.

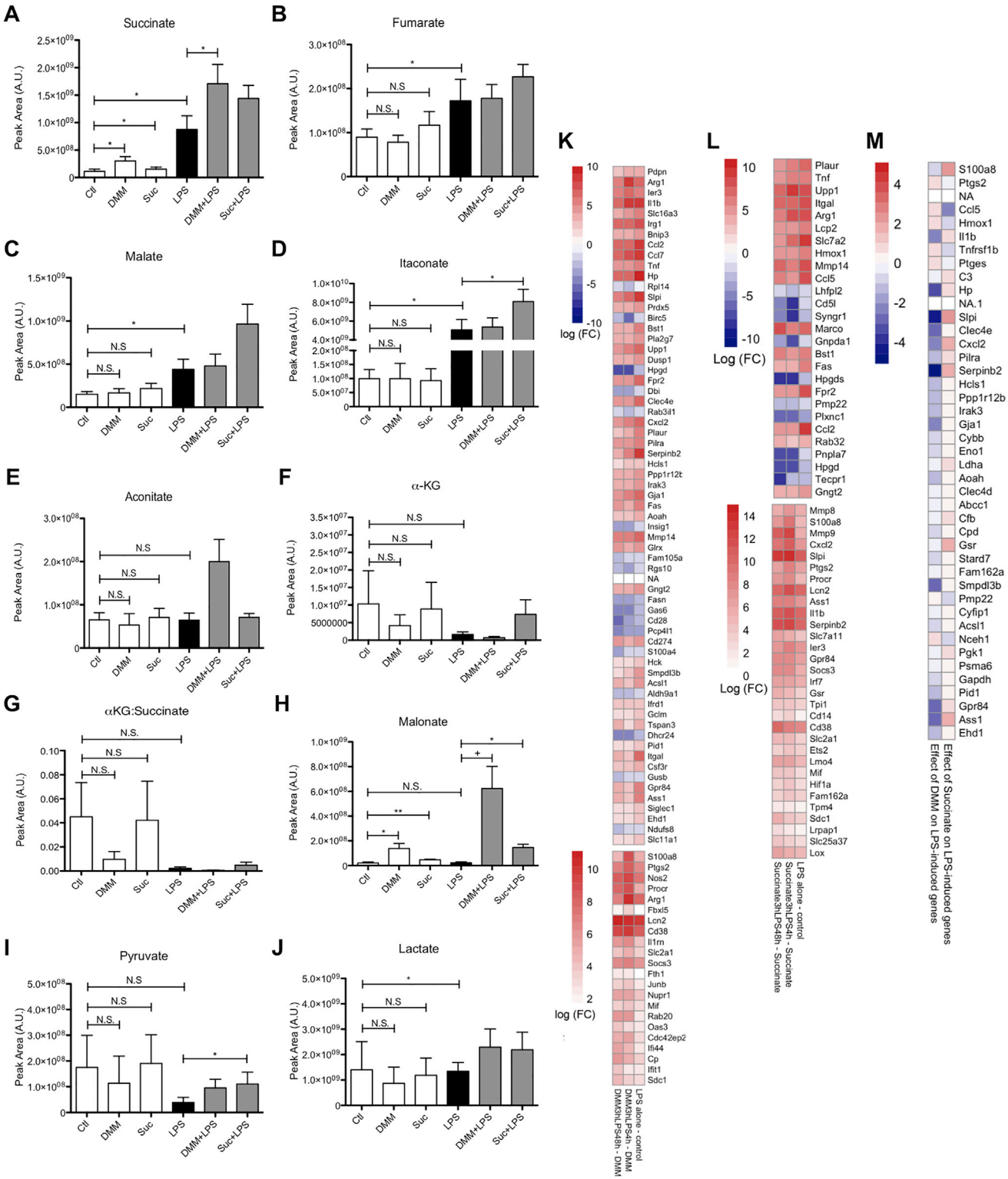

Figure S3. Succinate and Dimethyl Malonate Alter Levels of Succinate and Malonate, but Not Those of other Krebs Cycle Metabolites, and Also Impact the Transcriptome in LPS-Activated Macrophages, Related to Figures 1, 2, and 3

(A–M) BMDMs were pretreated for 3 hr with dimethyl malonate (DMM; 10 mM) or succinate (Suc; 5 mM) prior to stimulation with LPS (100ng/ml) for 24 hr (A – J). Lysed cells were analyzed by liquid chromatography-mass spectrometry (LC-MS) to determine metabolite levels. The data represent mean ± SEM, n = 3. +p = 0.05,

(legend continued on next page)

*p < 0.05, **p < 0.01. BMDMs were pretreated with dimethyl malonate (DMM; 10 mM) or succinate (5 mM) for 3 hr before being stimulated with LPS (100 ng/μl) for 4 or 48 hr (K – M). RNA was isolated and RNA sequencing was performed to determine genes significantly downregulated or upregulated by DMM (K) or succinate (L) and those that are most differentially regulated by DMM and succinate (M). The strength of the color refers to how strongly upregulated (red) or downregulated (blue) the various genes are.

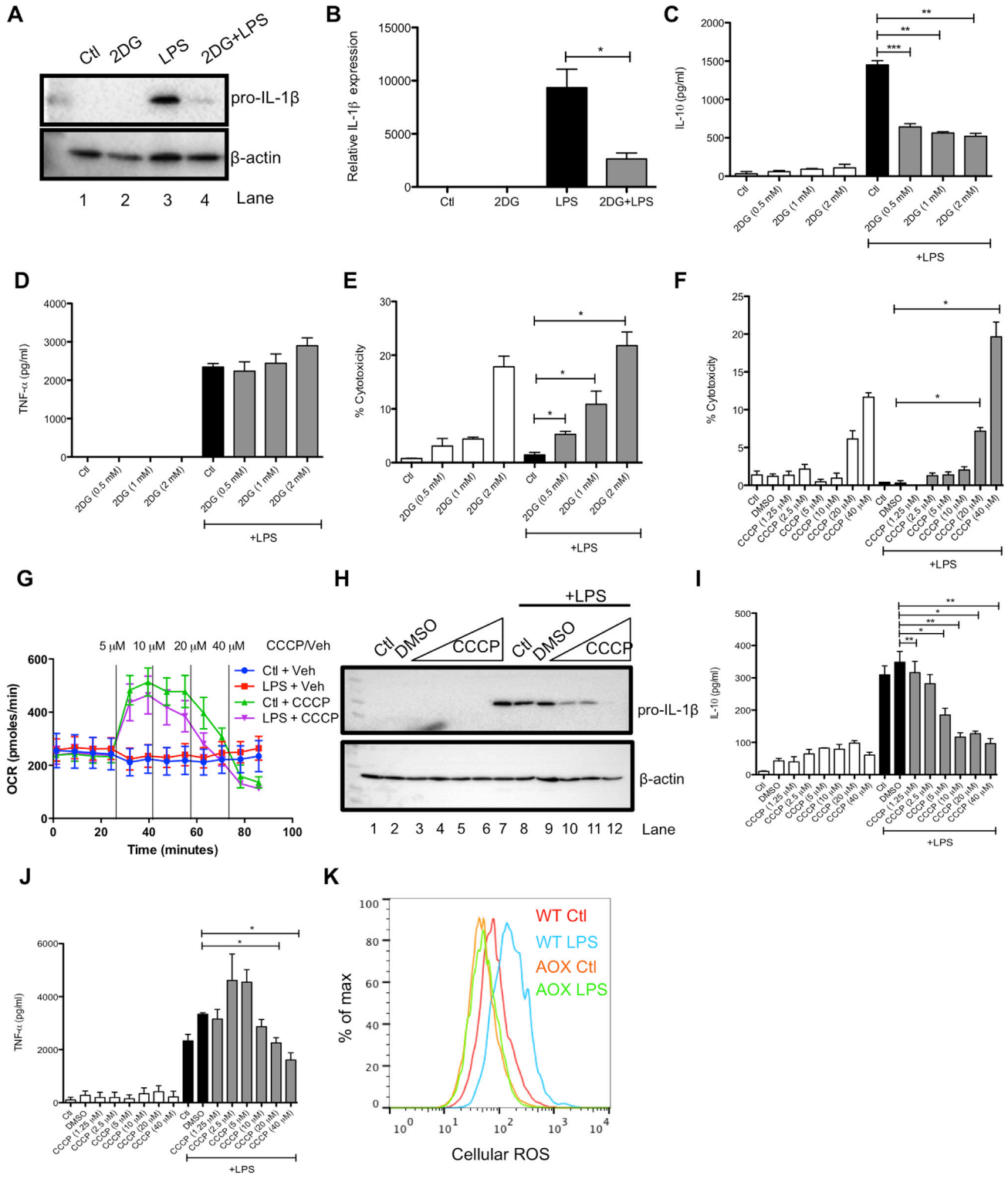

Figure S4. Dissipation of the Mitochondrial Membrane Potential by Inhibiting Glycolytic ATP Production or by Using CCCP Decreases LPS-Induced IL-1β, Related to Figure 5

(A–J) BMDMs were pretreated with 2-deoxyglucose (2DG; 0.5 - 2 mM) before being stimulated with LPS (100 ng/ml) for 48 hr (A – E), or were pretreated with CCCP (1.25 – 40 μM) before stimulation with LPS (100 ng/ml) for 4 hr (F, H, I). Whole cell lysates were analyzed by western blotting for pro-IL-1β and β-actin (A, H). mRNA was extracted from total cell lysates and analyzed by qPCR for IL-1β expression (B). Supernatants were analyzed by ELISA for IL-10 (C, I) and TNF-α (D, J)

(legend continued on next page)

production. % cytotoxicity was determined by a LDH release assay using a LDH-based cytotoxicity assay kit (E, F). The effect of increasing concentrations of CCCP on oxygen consumption (OCR) was analyzed using a Seahorse XF-24 analyzer (G). (K) Wild-type and AOX-expressing BMDMs were untreated (Ctl) or stimulated with LPS (1 μg/ml) for 48 hr. Live cells were analyzed by FACS and mean fluorescence intensity (MFI) was quantified as a measure of cellular reactive oxygen species production. The data in (B – F, I, J) represent mean ± SEM, n = 3, *$p < 0.05$, **$p < 0.01$, ***$p < 0.001$. The blots in (A, H) and the OCR data in (G) are representative of 3 independent experiments. The curves in (K) are representative of 5 independent experiments.

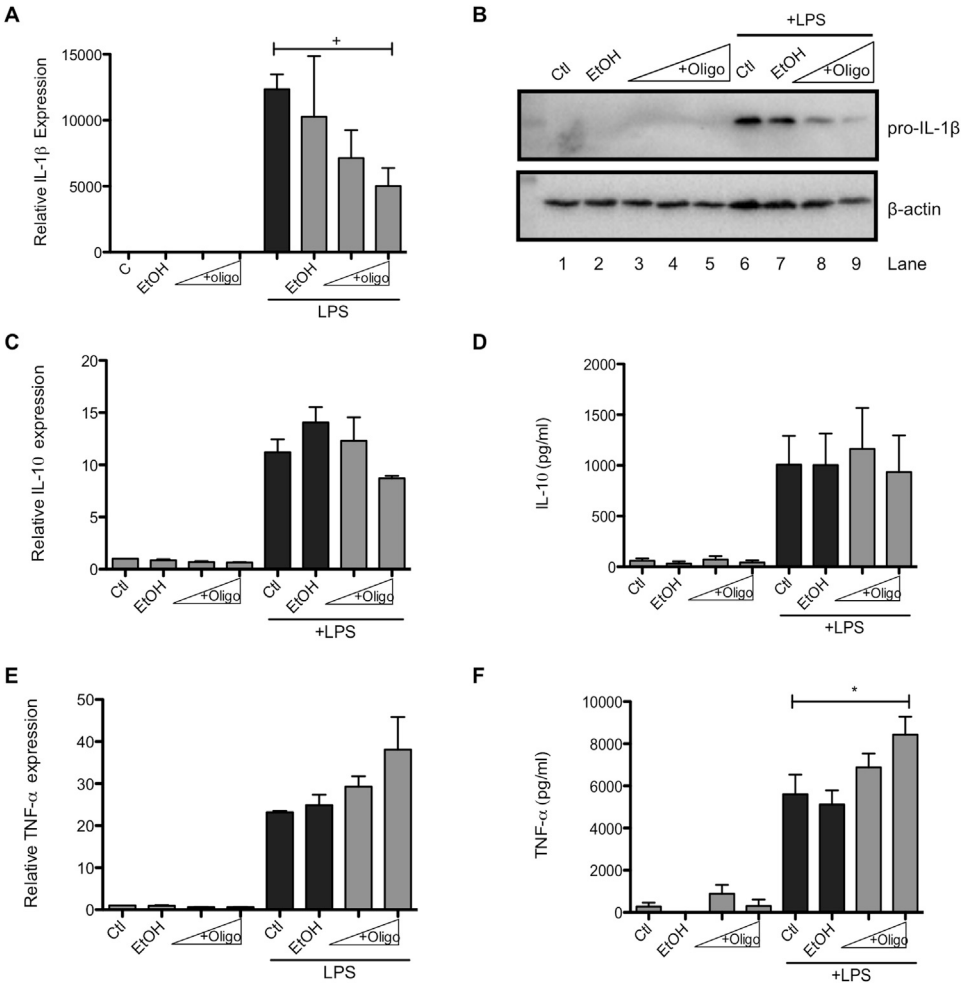

Figure S5. Inhibition of ATP Synthase with Oligomycin Decreases LPS-Induced IL-1β, Related to Figure 5

(A–F) BMDMs were pretreated with oligomycin (oligo; 1- 10 μM) before being stimulated with LPS (100 ng/ml) for 48 hr (A, B, D, F) or 4 hr (C, E). mRNA was extracted from total cell lysates and analyzed by qPCR for IL-1β (A), IL-10 (C) and TNF-α (E) expression. Whole cell lysates were analyzed by western blotting for pro-IL-1β and β-actin (E). Supernatants were analyzed by ELISA for IL-10 (D) and TNF-α (F) production. The data in (A, C - F) represent mean ± SEM, n = 3, *p < 0.05, + = 0.05. The blots in (B) are representative of 3 independent experiments.

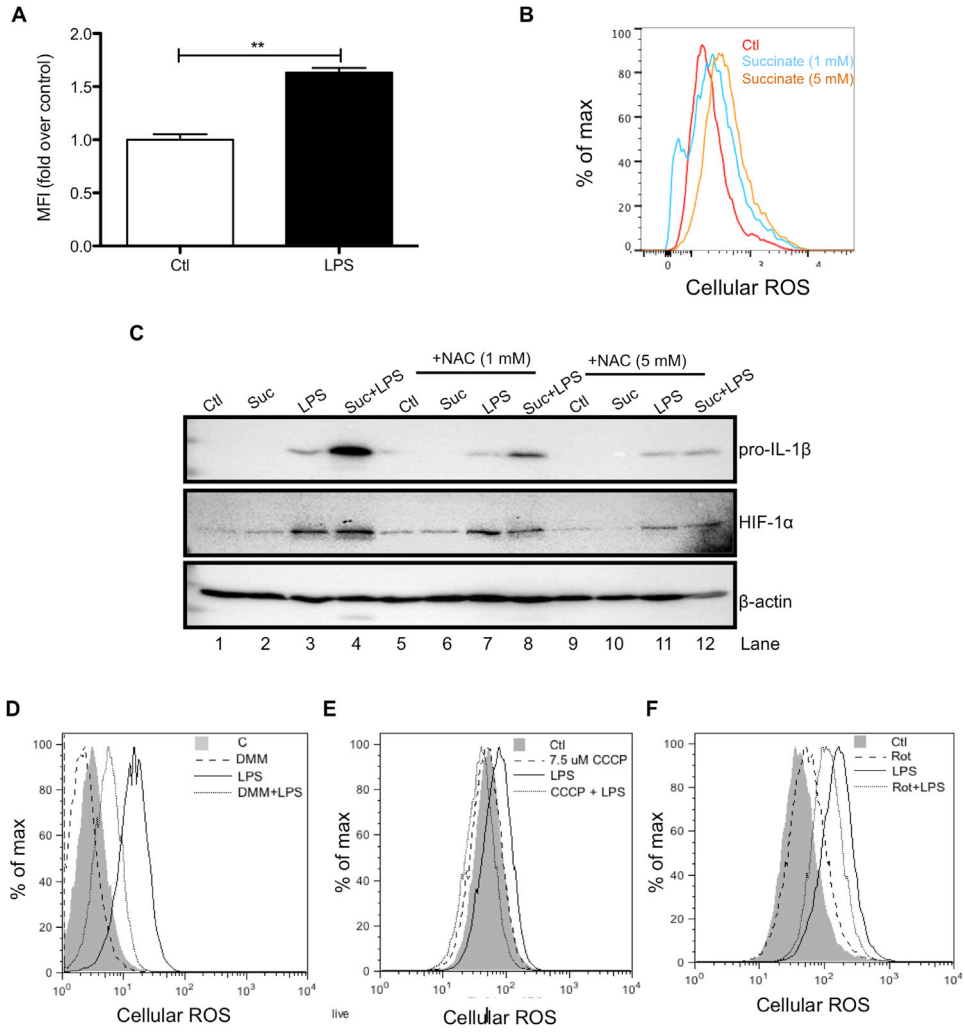

Figure S6. The Pro-Inflammatory Activity of Succinate Is ROS Dependent, while Inhibition of Complex I or II Activity or Dissipation of the Membrane Potential Limits ROS Production in LPS-Activated Macrophages, Related to Figure 6

(A–F) BMDMs were untreated (A), treated with succinate (Suc; 1, 5 mM) for 24 hr (B) or pretreated for 3 hr with dimethyl malonate (DMM; 10 mM; D), carbonylcyanide m-chlorophenylhydrazone (CCCP; 7.5 μM; E) or rotenone (Rot; 0.5 μM; F) before being stimulated with LPS (1 μg/ml; D – F) for 24 hr. Live cells were analyzed by FACS and mean fluorescence intensity (MFI) was quantified as a measure of mitochondrial (A) or cellular (B, D - F) reactive oxygen species production. BMDMs were untreated (Ctl) or pretreated with N-acetyl cysteine (NAC; 1, 5 mM) for 1 hr prior to the addition of succinate (Suc; 5 mM) for 3 hr before stimulation with LPS (100 ng/ml) for 48 hr. Whole cell lysates were analyzed by western blotting for IL-1β, HIF-1α and β-actin. The data in (A) represents mean ± SEM, n = 3, **$p < 0.01$. The curves are representative of 6 (B) or 3 (D - F) independent experiments. The blots in (C) are representative of 3 independent experiments.